BATTELLE
PACIFIC NORTHWEST NATIONAL LABORATORY

LIGO-C962289-00-D

FAX Transmittal

DATE:	September 19, 1996
SENT BY:	Alan Rohay
TO:	Rick Savage
COMPANY:	LIGO Project Caltech
FAX NUMBER:	818-304-9834
NUMBER OF PAGES (WITH COVER):	30

MESSAGE:

Rick

This is the first of two faxes - this one contains:

11 page report, 3 pages of figure captions, and figures 1-15

The second of two faxes contains: figures 16-36

Do whatever you can find time for to make any improvements. I sometimes am uncertain of the audience and so the level of detail or background may be way wide.

Alan

BOX 999
RICHLAND, WA 99352
509-376-6925
FAX 509-376-5368

Analysis of Differential Motions at the Hanford, Washington and Livingston, Louisiana LIGO Sites

Alan Rohay, Pacific Northwest National Laboratory

1.0 Introduction

Seismic measurements taken simultaneously at the Corner and two Ends of the Laser Interferometer Gravitational Wave Observatory sites provide the data needed to estimate the relative position differences between the Corner and each of the Ends. This analysis is conducted for data taken at the Livingston, Louisiana and Hanford, Washington, LIGO sites, where previous studies primarily described the motions at each measurement location independently from each other, and the analysis was conducted in the frequency range from 0.1 to 100 Hz. The analysis of the high-frequency vibrations primarily supported the design of passive vibration-isolation systems. In this study, the emphasis is on frequencies below 1 Hz, where active feedback systems may be used to maintain arm lengths within a prescribed tolerance.

A significant reduction of relative motion (compared to independent motions) is observed along the two perpendicular arms at the Hanford LIGO site. The reduction is greatest along the Northwest Arm, especially for the lower frequencies that comprise the largest ground motions. At Livingston, an increase in relative motion is determined, compared to that which would be expected from completely un-correlated motions at the different locations.

2.0 Data Description

Measurements were taken at the Livingston, Louisiana site from October 26 to November 2, 1995. These measurements were taken with three independently-operating seismometer and recorder systems that were synchronized to within 0.25 milliseconds using continuously-synchronizing GPS receivers. Earlier data collected at Hanford in 1994 were collected one location at a time, so synchronous data were collected there from January4-8, 1996 to provide the data for the current analysis. Data were sampled at 250 samples/second and 125 samples/second at Livingston and Hanford, respectively. For the purposes of this analysis of low-frequency correlation, both sets of data were decimated to a uniform 25 samples/second. A twelve-hour time series was analyzed for each of the two sites. At Livingston, the data used are from the period 1200 - 2400 GMT on Day 303 (6:00 a.m. CST to 6:00 p.m. CST on Monday, October 30, 1995). At Hanford, the data used are from the period from 0200 - 1400 GMT on Day 005 (6:00 a.m. January 4 to 6:00 p.m. January 5, 1996). The time period for the Livingston data was chosen because it represented a

period when the noise near 0.2 Hz was near the maximum observed during the recording period. At Hanford, the time period avoided complications from transient instrument irregularities.

The seismometers were oriented so that the "North" axis of the horizontal component seismometer was aligned with the LIGO arm nearest the north-south direction, as shown in Figure 1. Seismometers were calibrated before and after the deployments and system noise measurements were made that indicate the seismic noise is resolved above 0.1 Hz. The calibration results confirmed the responses measured by the manufacturer, showing that two of the instruments had an equivalent 20-second-period seismometer response and the third instrument had that of a 30-second-period seismometer. Although either response is sufficiently flat to ground velocity above 0.1 Hz, there is a slight phase response difference of the 30-second seismometer that was corrected to be the same as the two 20-second instruments.

The average vertical displacement spectra for the 12-hour period are shown for the three measurement locations at Livingston in Figure 2. Figures 3 and 4 show the spectra for the two horizontal components. Figures 5 through 7 shown the spectra measured at Hanford. The spectra from each measurement site generally overlie each other between 0.1 and 1 Hz. The Livingston spectra exhibit a broad peak just below 0.2 Hz, and the peak is higher on the horizontal components. At Hanford, the peak is much narrower and at lower frequency (near 0.13 Hz), and all three components have about the same amplitude. The noise measured at Hanford is significantly lower than at Livingston across most of the frequency range shown. The Hanford spectra show a uniform decrease in amplitude from 0.2 to 1 Hz. The Livingston spectra show secondary peaks near 0.3 and 0.7 Hz, particularly on the vertical spectra. These two higher-frequency, secondary peaks may be associated with different sources, potentially with sources in the Gulf of Mexico and Lake Pontchartrain, respectively.

Appendix A contains a set of color spectrograms that illustrate the temporal variation in the noise (ground motion in terms of velocity) from 0.1 to 1 Hz.The spectrograms show the amplitude of ambient noise color-coded as a function of frequency and time. Spectra are taken from 180-s windows that are shifted 90-s. Each plot shows the spectra for a 24-hour period, when available. For the Hanford site, data are shown from one day at each of the three measurement sites occupied in the 1994 deployment in addition to the 12-hour period in 1996 when the simultaneous measurements were taken.

3.0 Noise Model

Ambient seismic noise measured on land in the frequency range 0.1 - 1 Hz is usually dominated by a noise peak near 0.15 - 0.2 Hz, termed the "microseism" or "microtremor" noise. Seismic array studies indicate that the microseism noise is usually generated where large storm wave hit particular beaches, but can also be generated from sources in the deep ocean. There are several proposed mechanisms for the generation and propagation of microseisms, generally involving the interaction of ocean waves travelling in different or opposite directions that establish a standing-wave pattern. Such effects can occur near a

coastline or beach that is capable of reflecting a set of waves without much loss, or when sets of ocean waves from different storms interact.

Three-component polarization and array analysis of seismic data indicate Rayleigh-wave propagation at velocities near the average crustal shear-wave velocity (near 3.5 km/second). It has been observed that the average microseism noise is higher in the northern latitudes during the first and fourth quarters of the year, when storm activity is more frequent and intense.

Rayleigh waves travelling at 3.5 km/s with periods ranging from 6 to 8 seconds (corresponding to the peak noise frequencies observed at Livingston and Hanford, respectively), have wavelengths of 21-28 km. This is 5 to 7 times longer than the 4 km arms of the L-shaped array formed by the LIGO measurement locations, implying a phase delay of 70 to 50 degrees, respectively. Assuming purely sinusoidal motion, these phase delays will affect the displacement differences by +15% and -15% for the shorter (6-second) and longer (8-second) period waves for two locations separated by 4 km parallel to the wave-propagation direction. Variation in the direction of wave approach can result in one End and the Corner being in-phase (along the arm that is perpendicular to the wave-propagation direction), while the other End and Corner (along the arm parallel to the wave-propagation direction) will be out of phase by the above amounts. This model of propagating waves indicates that a reduction or at most a modest increase should result when differential motions are compared to the independent motions at each end of an arm. Longer periods and wavelengths reduce phase differences.

The geography of the Hanford LIGO area suggests that the microseism noise will be dominated by sources located on the Pacific coast or more distant sources within the Pacific Ocean, and will therefore arrive from a broad range of generally western azimuths. The lower-frequency (0.125 Hz) peak in the amplitude spectrum will tend to reduce the phase differences and differential displacements by at least 15% The seismic velocity structure is well known at Hanford and a Rayleigh-wave velocity near 3.5 km/second is appropriate in this frequency range. Assuming propagation from western azimuths (approximately 45 degrees to both of the LIGO arms), the differential motion along both arms should be reduced by a total of 40% relative to independent motion.

The geography of the Livingston LIGO area suggests that the microseism noise might be generated from sources in the Gulf of Mexico, although sources in the more distant Atlantic Ocean are also expected. Wind-generated waves in Lake Pontchartrain could also generate a "lake-effect" that might be observed at Livingston.There may be significant differences in how microseism waves are generated and propagated from these potential sources because of the differences in the areas and depths of the water bodies, and in the characteristics of shorelines bordering them. The geologic structure is known to be dominated by a thick sedimentary sequence at shallow depths implying low seismic velocities in the uppermost 5 km, but is very poorly known at greater depth. The above factors make a prediction of the expected microseism directions variable and velocities uncertain. The shorter period (6 seconds) of the peak amplitude spectrum at Livingston and the indication of lower seismic velocities in the region suggests that a modest increase in differential motion relative to independent motion may result. Assuming a lower Rayleigh-wave

velocity of 2 km/second for the peak noise at 6 seconds, the phase difference is 120 degrees for a 4-km separation, suggesting that differential motion would be 70% larger than the independent motions.

4.0 Wavenumber Analysis

A wavenumber analysis conducted on the measured signals at the two sites indicates substantial differences in the structure of the noise wave field at the two sites. At the Hanford site, fast-propagating waves consistent with Rayleigh wave propagation are observed, but there are many periods when higher velocities are observed that are more typical of body waves. Sources from westerly directions are frequently observed, as expected, but waves arriving from northeastern directions are also observed. At Livingston, wave propagation velocities are concentrated at lower velocities near 2 km/s, and the dominant direction of approach is north-northwest. At Hanford, particular wave shapes observed in the time series can be tracked from location to location, but this is not the case at Livingston, where wave shapes have different appearances. This may be indicative of an interference pattern from sets of waves crossing the array from different directions, but this cannot be resolved with just the tripartite array formed by the three measurement locations. The dissimilar wave shapes, combined with large phase differences (approaching 180 degrees) make interpretation of the wavenumber results ambiguous at Livingston. To insure that the data were properly taken and analyzed at Livingston, the following analysis of a series of fast-moving waves from a distant earthquake is presented, which provides an introduction to the wavenumber method used.

Analysis of earthquake signal correlation. The timing and response of the three measurement installations at Livingston can be demonstrated to be empirically correct by analyzing the signals from a distant earthquake. The earthquake had a magnitude of 6.4 and was located near the coast of central Chile (28.9 S, 71.4 W) on Day 305 at 00:35:32 GMT. Positive polarity compressional waves are expected at Livingston, and a standard earth velocity model predicts an apparent velocity of 16 km/second (the waves arrive from a near vertical inclination) from an azimuth of 161 degrees. This practically coincides with the orientation of the South Arm of the LIGO facility, so it implies that the South End should detect these waves in advance of the Corner by 0.25 s, and the West End should detect these waves simultaneously with the Corner.

Figure 8 shows the time series from all three vertical-component channels (the lower plot shows the corrected response of the 30-s seismometer). This plot clearly illustrates the consistency of the earthquake signals. (It also shows an example of the lack of coherence of the noise preceding the arrival of the earthquake signals.) Other sections of the earthquake signal were also examined for the three north-south and three east-west channels to insure that all signals had the correct polarity and amplitude.

The wavenumber analysis attempts to determine the vector velocity of a plane wave crossing the array formed by the three sensors. The analysis projects the power of the combined three signals onto the two-dimensional wavenumber plane. The peak power on the wavenumber plane is then selected to represent an azimuth of approach and a propagation

velocity. A segment of the three vertical signals was taken and the ends of the segment were tapered to zero to remove end effects for the subsequent two-pass (forward and reversed) band-pass filtering.

Wavenumber analyses for two filter bands, from 0.1 to 0.2 Hz and from 0.8 to 1.0 Hz, are shown in Figure 9, where the combined power of the three signals is contoured as a function of the two horizontal wavenumbers. The peak amplitude occurs at 0.008 and 0.035 cycles/km. The propagation velocity is determined by the ratio of the peak frequency f (in cycles/s or Hz) and the wavenumber k (in cycles/km) using v = f/k. The velocity determined for the two analyses is 19-25 km/s, for comparison to that predicted, 16 km/s. The azimuth estimated from the wavenumber diagrams is from an eastern or southeastern direction, compared to the predicted southeastern azimuth of 161 degrees.

Direct measurements of time delays between earthquake signals from signal cross-correlation indicate that the South End was advanced relative to the Corner by only 0.16 s, but that the West End was also delayed by 0.12 s relative to the Corner. This implies a travel time over a 4 km distance equal to the geometrical sum of the delays (sqrt(0.16^2 + 0.12^2)) or a 4-km travel time of 0.2 s. Using simple geometry, the result is that the signals are crossing the array at 20 km/s from an azimuth of 125 degrees, in approximate agreement with the higher-frequency wavenumber result. Similar results were obtained using other portions of the earthquake signal as recorded on the horizontal components.

It is common for earthquake travel times to be systematically delayed or advanced by 0.1 s at different locations, but there are no significant elevation differences between the three measurement locations, nor any significant seismic velocity differences expected beneath these locations. This suggests that there are physical and/or numerical limits to the noise correlation results within a resolution of 0.1 s, but his is a relatively small portion of the period and expected transit time of observed microseisms.

Wavenumber analysis of peak microseism noise. The amplitude spectra at Hanford and Livingston indicate that the microseism peak occurs at different frequencies at the two sites. At Hanford, a sharp peak is consistently near 0.12 Hz (8 second period). At Livingston, a broader peak is observed between 0.15 and 0.2 Hz (5-7 second period). The wavenumber analysis is designed to focus on a narrow frequency band at the peak frequency at each of the two sites. Frequency bands of 100-150 mHz and 150-200 mHz were appropriate for a comparative analysis of the maximum noise peak at Hanford and Livingston, respectively. The analysis was conducted using both frequency bands at each site for comparison. Only the vertical channel has been analyzed, because the amplitude changes with wave direction when dominant horizontal polarization exists (as is expected for Rayleigh wave propagation). Filtering in these two bands was done with a 2-pole Butterworth filter operated on both the forward and reversed time series to eliminate the filters' phase shifts. Filtering was conducted on one-hour data segments with the first and last 0.5% (18 seconds) tapered to zero to eliminate filter transients.

The one-hour filtered data were then windowed into overlapping 60-s segments using a squared, raised cosine bell to strongly enhance the middle 30 s of the data. This obtains 4-5 cycles of the noise for each wavenumber measurement. The window was shifted 30 s for

each subsequent measurement. The windowed time series amplitudes were normalized so that the peak amplitude output of the wavenumber analysis at Hanford was approximately unity for the 100-150 mHz band.

The wavenumber analysis selects the peak power on the two-dimensional wavenumber plane to represent the azimuth of approach and propagation velocity. The search for the peak power was restricted to a wavenumber k (in cycles/km) less than the highest frequency f (in cycles/s or Hz) of the filter pass band. The slowest velocity allowed is thus 1 km/s, given the rule f/k >1 km/s. The restriction to propagation velocities less than 1 km/s is partially based upon the expected propagation velocity, but there can remain ambiguity in the determination of the direction and propagation velocity within this limit.

Figure 10 shows two examples of wavenumber analyses at Hanford. The example on the left shows a time segment when all three signals were practically identical in phase, resulting in the central peak at zero (infinite apparent velocity and therefore inconsistent with horizontally-propagating Rayleigh waves). The example on the right shows the opposite extreme, where two peaks are observed with nearly equal wavenumbers having azimuths separated 180 degrees from each other. The ambient noise at the Southwest End and Corner during this time segment are out of phase by 180 degrees, and the Northwest End and Corner are nearly in phase. The wavenumbers for either peak are near 0.125 cycles/km, and from the frequency of 125 mHz, a propagation velocity of 1 km/s along the either direction of the Southwest arm results (which is much slower than expected for Rayleigh waves). This situation simply corresponds to a time delay/advance of 4 s, half of the 8-s period.

At Livingston, where the frequency is higher, near 185 mHz, it is more difficult to select the correct maximum on the wavenumber plane. Figure 11 shows two examples of the wavenumber analyses there. The contour diagram on the right has a unique (closest to zero) peak on the wavenumber plane, and choosing this as the correct value, a velocity near 2 km/s is determined (the wavenumber near 0.09 cycles/km). This example (the right side of Figure 11) is the typical result at the Livingston site. The phase at both Ends is delayed equally by 1.4 s relative to the Corner in this example.

The example on the left side of Figure 11 shows a similar example, but in this case, there can be alternative choices within the limitation f/k>1. The two maxima have wavenumbers near 0.14 cycles/km and so a velocity of approximately 1.3 km/s results, either in a northerly or a southeastern direction. If even slower velocities are considered possible, then the two maxima on the left half of the wavenumber plane could also be correct. There are maxima in the wavenumber plane separated every 0.25 cycles/km in directions parallel to the two 4 km arms of the tri-partite arrays, and this cyclic effect (termed beam-pattern), represents potential full-cycle jumps in the cross-correlation of the signals.

Using the f/k >1 restriction eliminates most situations where the peak selected from the wavenumber analysis aligns the noise signals with phase shifts greater than 180 degrees. A more restrictive limit can, however, produce biases because of the "flatter" aperture of the array in the direction parallel to the bisector of the two arms. For example, the phase relationships intermediate to those that produced the wavenumber diagrams in Figure 11 will

preferentially pick a northeastern azimuth of wave approach if a restriction to velocities higher than 1 km/s are considered. A trade-off exists between attempting to fit the data to a model that predicts fast propagation velocities versus a model that suggests southeastern azimuths as possible sources for the noise.

Wavenumber results at Livingston. Figure 12 shows the result of the wavenumber analysis for the Livingston site in the frequency band 0.15 - 0.20 Hz. At Livingston, the noise is naturally peaked in this frequency range. The three plots on the left of Figure 12 show the temporal distribution of the 12-hour, moving-window wavenumber analysis. The uppermost of these plots shows the azimuth estimate, the middle shows the wavenumber estimate, and the lower shows the peak amplitude of the wavenumber analysis. A slight variation in amplitude over time reflects the overall amplitude variation observed on the spectrograms in Appendix A. The azimuth of wave approach is most frequently from a north or northwest direction (azimuth 0-45 degrees), with azimuths near 135 and 270 degrees occurring less frequently. The middle plot on the left rarely shows wavenumbers less than 0.05 cycles/km and wavenumbers range from 0.05 to the maximum, 0.20 cycles/s with no concentrations at any particular value.

The top plot on the right of Figure 12 shows that most of the low-wavenumber results are associated with the north-northwest approach directions, and the azimuth determinations that cluster near 135 and 270 are associated with the largest wavenumbers (see Figure 11). It is these latter situations (large wavenumbers) that would indicate slow propagation velocities, large phase differences, and ambiguous phase determinations. The middle plot on the right of Figure 12 shows that the amplitudes of the wavenumber results outside of the three azimuth groups are systematically lower than those within the three azimuth groups. The lower plot on the right shows the amplitude distribution as a function of the wavenumber, and here there is a slight tendency for wavenumbers near 0.10 and from 0.15-0.20 cycles/km to have higher amplitudes.

The most significant result of this analysis is that there are very few instances where the wavenumber of the dominant noise field is less than 0.05 cycles/km. The wavenumber is most frequently near 0.1 cycles/km (and frequently higher), so that the noise propagation velocities are interpreted to be near 2 km/s or lower, given that the dominant frequency is below 0.2 Hz (the peak is near 185 mHz). The low-wavenumber results are primarily associated with a direction of approach of north-northwest. This result is inconsistent with the expected sources in the Atlantic Ocean or other possible sources such as the Gulf of Mexico. The analysis consistently indicates that large phase differences exist, and by restricting the result to minimize the phase differences, the north-northwest direction results. This direction is approximately 45 degrees from the orientation of the two arms, indicating that the Corner is out of phase from either End by about the same amount (1.5 s). For a wavenumber of 0.1 cycles/km, the phase difference is approximately 100 degrees.

Figure 13 shows the results of a wavenumber analysis for the Livingston data when the time series are filtered to a lower frequency range, 100-150 mHz. This is below the peak frequency analyzed above, so the amplitudes of the wavenumber results are lower, but similar results are still found. The azimuths are consistently in the north-northwest direc-

tion, and the wavenumbers cluster near 0.05-0.07 cycles/km. This again implies propagation velocities near 2 km/s.

The wavenumber results at Livingston are considerably different from the model of propagating plane waves with velocities above 3 km/s from source regions in oceans or seas. If propagation velocities are instead actually as low as 1 km/s, the wavenumber results could possibly admit nearly 360 degree phase differences between the two Ends, and intermediate (180 degree) phase differences at the Corner, with propagation from an azimuth of approximately 120 degrees. The azimuth of 120 degrees would appear to be consistent with sources in the Gulf of Mexico, but the propagation velocity required is considered unrealistically low. As noted previously, If the relative phase of the noise is completely random, a concentration of azimuths that bisect the two arms (in the north-northeast or south-southwest) directions could occur when the wavenumber estimate is limited to a small value (maximizing the velocity). The azimuth distribution determined for the Livingston data is consistent with one of these two directions, but the stronger concentration of azimuth estimates from north-northeast directions suggests that the unequal array aperture is not completely controlling the result.

Wavenumber results at Hanford. Figure 14 shows the wavenumber results at Hanford for the peak noise frequency 100-150 mHz. The three plots on the left show the temporal distribution of, from top to bottom, the azimuth, wavenumber, and amplitude of the wavenumber analysis. The azimuth of approach of the peak noise is appears to be from a wide, generally westerly azimuth range from 180 to 360 degrees, with an additional concentration near a northeastern azimuth of 45 degrees. There appears to be an increasing frequency of the northeastern azimuth in the later portion of the time period. The wavenumbers appear to be centered near 0.035cycles/km. Using the peak frequency of the noise in this range (125 mHz), the velocity determined from the relationship $v = f/k$ is 3.5 km/s.

Figure 14 also shows, on the right half of the page, that the wavenumber distribution (top) and the amplitude distribution (middle) are similar for either the northeastern or the western azimuths. The bottom plot shows that the higher amplitude wavenumber results (those with high signal coherence) are concentrated for the wavenumbers below 0.05 cycles/km.

Figure 15 shows the results of the wavenumber analysis at Hanford in the higher frequency band 150-200 mHz, above the peak frequency at Hanford but at the peak frequency observed at the other site at Livingston. Similar results are found as for the lower frequency band at Hanford, with amplitudes reduced by the fall-off of the underlying noise spectrum.

The wavenumber results at Hanford are generally consistent with the expected model of propagating wave with velocities near 3.5 km/s from sources in the Pacific Ocean. However, there are many periods where higher and slower velocities are observed, and there is an additional source of noise that appears to propagate across the site from the northeast.

Histograms of wavenumber results. Figures 16 and 17 show histograms of the azimuth and wavenumber results for the Hanford and Livingston sites. Comparison of the azi-

muthal distributions at Hanford for the 100-150 mHz and 150-200 mHz bands indicates that the peak azimuths are near 30 and 230 degrees in the lower (peak) frequency band, but that the azimuth in the higher frequency band is peaked more strongly for the 30 degree azimuth. The azimuth distribution at Livingston is concentrated near 20 degrees, except for the secondary groups near 120 and 280 degrees that were associated with large wavenumbers and phase shifts approaching 180 degrees.

The peak in the wavenumber distribution at Hanford for the peak frequency band (100-150 mHz) is frequently as low as 0.02 cycles/km, implying propagation velocities are frequently as high as 6 km/s. The range of frequently-estimated wavenumbers from 0.01 to 0.04 cycles/km indicates a range of propagation velocities from 3 to 12 km/s.

At Livingston, the peak in the wavenumber distribution is found at 0.07 and 0.11 cycles/km for the lower and higher frequency bands, respectively. These wavenumbers correspond to propagation velocities near 2 km/s. The range of wavenumbers observed for the lower frequency band (100-150 mHz) is 0.04 to 0.11 cycles/km, indicating a range of propagation velocities from 1 to 4 km/s.

5.0 Differential Motions

The r.m.s. difference in position of the Corner and End stations is determined in three one-octave frequency bands, using a sample length that corresponds to one cycle of the lowest frequency in the band or two cycles of the highest frequency, as shown in the table below.

Frequency Band (Hz)	Sample Length (s)	Number of Samples
0.1 - 0.25	8	5400
0.25 - 0.5	4	10800
0.5 - 1.0	2	21600

The lowest frequency band includes the peak amplitude of the ambient noise spectra at the Hanford and Livingston LIGO sites that were analyzed for correlation in the previous section. The processing of the data for calculating the position differences from the recorded signals is similar to that used for the wavenumber analysis, using one-hour segments of 25 samples/s time series that have had the first and last 0.5% tapered to zero to avoid transient effects (18 s of data at the start and end of each hour are affected). Note that this tapering will affect the extreme tail of the distribution of small displacements but does not significantly affect the distribution of displacements above 99% probability of exceedance (it can randomly remove up to 1% of the population of higher displacements).

The tapering above was also necessary to eliminate transients from the conversion of the 30-s seismometer to be identical to the two 20-s seismometers. The gain factor for each time series was applied to obtain ground velocity from the digitally-recorded seismometer outputs. Band-pass filters were applied to each one-hour time series, using the same filter types as above (2-pole Butterworth filters passed twice over the data, once in a forward direction and once in a reversed direction). The effect of the band-pass filters on a sample

spectrum from Livingston is shown in Figure 18. After filtering, the time series is integrated to obtain ground displacement from the velocity time series.

The Corner-to-End difference between the displacement time series was determined for each component of the seismometer systems. The vertical difference corresponds to a vertical tilting of the two arms. The north difference corresponds to an arm-parallel displacement or strain of the Northwest Arm at Hanford or the South Arm at Livingston (see Figure 1), and rotation of the perpendicular arms (about a vertical axis). The east difference similarly corresponds to an arm-parallel displacement of the Southwest Arm at Hanford or the West Arm at Livingston.

Comparison of differential motions to independent motions. Figures 19 to 24 show histograms of the ratio of the r.m.s.displacement differences to the r.m.s. of the two contributing independent motions. The value of this ratio can range from 0 to 2, if the two displacement time series are identical or opposite. Two completely random signals are expected to have an average value near 1.4. At the bottom of each histogram are two triangles marking the mean and median value of the ratios.

The distributions of ratios for the vertical motions at Livingston are shown in Figures 19. In the two higher frequency bands (250-500 and 500-1000 mHz), the mean and median values are near the value expected from the difference between two un-correlated time series. The ratios for the lowest frequency band (100-250 mHz), where the motions are largest, are slightly higher than this value. This is consistent with the results of the wavenumber analysis that was conducted within this frequency range. The wavenumber analysis of the vertical channel most frequently detected phase differences near 100 degrees between the Corner and the two Ends. The ratio of r.m.s. differences formed from two equal-amplitude sinusoids with this phase offset of 100 degrees is 1.5, as compared to 1.4 if the phase difference is just 90 degrees.

The distributions of ratios for the horizontal motions at Livingston are shown in Figures 20 and 21. The east-component distributions are similar to the vertical channel, and the north component distributions are similar except for a slightly increased ratio (up to 1.6) in the low- and intermediate-frequency bands for the West Arm (this is motion perpendicular to this arm or a rotation of the arm). In the low band, the South Arm has a ratio near 1.4 instead of the higher value of 1.5 observed for the vertical and east components.

Figure 22 shows that at Hanford, significant reductions in differential motion result, particularly for lower frequencies and for the Northwest Arm. This is consistent with the wavenumber analysis that showed small phase differences or high propagation velocities across the array. The reduction of differential motion relative to independent motion is stronger on the Northwest Arm, which is perpendicular to one of the principal azimuths (from the northeast) determined in the wavenumber analysis, so the phase difference is smaller during those periods when this azimuth is dominant. Figures 23 and 24 show the ratios for the north and east components, which show similar results, except that the north-component differences are higher than 1.4 for along the Southwest Arm (again, this is motion perpendicular to this arm or a rotation of the arm).

Differential Motion Histograms. The final set of twelve figures, Figures 25 through 36, show the cumulative exceedances of r.m.s. differential displacements in the three frequency bands and set of sampling windows used above. Each figure displays the cumulative distribution of r.m.s. displacement for each of the contributing independent motions and their differences, for each of the three frequency bands. A complete description of the differential motions in three directions (vertical tilting, arm-parallel stretching, and horizontal rotation) is provided for Livingston (Figures 25 to 30) and Hanford (Figures 30 to 35). For both sites, the largest displacements are found in the 100-250 mHz band.

At Livingston differential displacements exceed 10^{-6} m approximately 90% of the time for the horizontal motions, and approximately 30% of the time for vertical motions in the low-frequency band. The slightly larger ratios of differential to independent motions at low frequency is only subtly visible in these diagrams. In the higher frequency band (500-1000 mHz) at occurrence rates below 1%, the plots show the effect of another earthquake (a magnitude 5 event from southern Mexico) that occurred during the 12-hour period analyzed. The earthquake ground motions have a significant effect on the horizontal motions.

At Hanford, differential displacements rarely exceed 10^{-6} m in the low-frequency band. The reduction of differential motion relative to independent motion is apparent especially for the Northwest Arm in the low-frequency band. Along this arm there were many periods that were observed to have high signal coherence that the wavenumber analysis detected as propagation in a direction perpendicular to this arm.

6.0 Conclusion

The microseism noise, peaked in amplitude near an 8 s period at Hanford and between 5-6 s period at Livingston, produces the largest displacements at the two LIGO sites. This noise is expected to be produced from oceanic or coastal areas and to propagate at velocities near the average shear-wave velocity of the earth's crust, approximately 3.5 km/s. This model should produce a reduction or at worst a slight increase in the amplitude of differential motions between the End stations and the Corner because of the long wavelengths implied. However, at both Hanford and Livingston, the observed phase relationships between measurement sites are not wholly consistent with this simple model.

At Hanford, wavenumber analysis frequently indicates velocities near 3.5 km/s from western azimuths that would be appropriate for sources in the Pacific ocean or along the coast. But there are also many periods when a northeast azimuth is determined, and many periods when significantly higher velocities are determined. The periods when a northeast azimuth is determined is the result of coherent noise at the Northwest End and Corner, which significantly reduces the average differential motion along this arm. At Hanford, the generally high velocities confirm the expected reduction in Corner-to-End differential motion relative to that expected from un-correlated motions at the three measurement locations. This reduction is effective in the frequency range that the peak microseism amplitudes are observed, but the microseism vibrations become progressively less coherent at higher frequencies.

At Livingston, the phase relationships between the Corner and Ends indicate unexpectedly slow velocities (near 2 km/s) for propagation of microseism noise, and a direction of propagation that does not correspond to sources near coasts or in the oceans. The slow velocity may result from a thick layer of sediments, but the velocity structure of this region is not well known. If velocities lower than 1 km/s are possible for these low-frequency waves, other azimuths are also possible. It is also possible that patterns of interfering waves frequently establish stable phase relationships between the Corner and Ends that do not necessarily correspond to the actual propagation direction of the components of the wave field. Although the results at Livingston indicate larger phase differences between the Ends and the Corner than expected, they only modestly increase the average ratio of differential motions to independent motions relative to that expected for completely random signals (a ratio of 1.6 compared to the expected ratio of 1.4).

The difficulty in characterizing the propagation modes of microseism noise from 0.1 to 1 Hz is because the array geometry is suitable only for wavelengths longer than the spacing between measurement locations. In order to determine whether multiple signals might be present in the wave field, more than three measurement locations must be occupied. The anomalously slow wave velocities implied by the wavenumber analysis at Livingston suggests that the propagation characteristics of the microseismic noise there may not be consistent with previous characterizations of this noise as fast, long-wavelength Rayleigh waves.

Figure 1. Orientation of seismometer components at LIGO sites at Livingston and Hanford.

Figure 2. Livingston vertical-component amplitude spectra. Each spectrum is an average of 12 spectra computed from one-hour samples. The Corner, South End, and West End are overlaid.

Figure 3. Livingston north-component amplitude spectra. Each spectrum is an average of 12 spectra computed from one-hour samples. The Corner, South End, and West End are overlaid.

Figure 4. Livingston east-component amplitude spectra. Each spectrum is an average of 12 spectra computed from one-hour samples. The Corner, South End, and West End are overlaid.

Figure 5. Livingston vertical-component amplitude spectra. Each spectrum is an average of 12 spectra computed from one-hour samples. The Corner, South End, and West End are overlaid.

Figure 6. Livingston north-component amplitude spectra. Each spectrum is an average of 12 spectra computed from one-hour samples. The Corner, South End, and West End are overlaid.

Figure 7. Livingston east-component amplitude spectra. Each spectrum is an average of 12 spectra computed from one-hour samples. The Corner, South End, and West End are overlaid.

Figure 8. Time series from Chilean earthquake recorded on vertical components at Livingston LIGO site.

Figure 9. Wavenumber results from compressional wave window for Chilean earthquake.The contour plots show the combined power of the three vertical-component signals contoured as a function of wavenumber in the two horizontal directions. Left contour plot is for earthquake signals band-passed from 100-200 mHz. Right contour plot is for 800-1000 mHz.

Figure 10. Examples of wavenumber results for vertical-component ambient noise at Hanford. The frequency band is 100-150 mHz (the peak noise band). The plot on the left shows a result with "infinite" apparent velocity, indicating all three signals are in-phase (as might result of a vertically-propagating body wave). The plot on the right shows a result where there is nearly a 180-degree phase shift at the Southwest End relative to the Corner and Northwest End. Propagation velocity implied is 1 km/s. A 180-degree phase shift corresponds to a wavenumber of 0.125 cycles/km for the peak frequency of 0.125 cycles/s. The wavelength is twice the arm length, and the time-delay is half the period. The propagation direction could be from the northeast or from the southwest.

Figure 11. Examples of wavenumber results for vertical-component ambient noise at Livingston. The frequency band is 150-200 mHz (the peak noise band). The plot on the left shows a result with two peaks on wavenumber plane that are nearly equidistant from the origin. The wavenumbers corresponding to these peaks are near 0.15 cycles/km, implying a velocity near 1 km/s. Interpretation as propagation at this slow velocity from north-northeast or southeast directions. Lower velocities are implied by the peaks at west-northwest and southwest azimuths. The plot on the right shows a typical result at Livingston, where the peak on wavenumber plane 0.85 cycles/km from the origin implies a velocity near 2 km/s and a preferred azimuth from the northeast.

Figure 12. Wavenumber results for the twelve-hour period at Livingston for the frequency band 150-200 mHz containing the peak noise amplitudes.

Figure 13. Wavenumber results for the twelve-hour period at Livingston for the frequency band 100-150 mHz, lower than the peak noise amplitude band.

Figure 14. Wavenumber results for the twelve-hour period at Hanford for the frequency band 100-150 mHz containing the peak noise amplitudes.

Figure 15. Wavenumber results for the twelve-hour period at Hanford for the frequency band 150-200 mHz, higher than the peak noise amplitude band.

Figure 16. Histograms of azimuth and wavenumber results at Hanford.

Figure 17. Histograms of azimuth and wavenumber results at Livingston.

Figure 18. Effect of band-pass filters on an example spectrum. Spectra are averages of 39 spectra taken within a one-hour time sample at Livingston. Plot superimposes spectra from the unfiltered and three band-passed time series. The filters are two-pole Butterworth filters that operate twice (forward and backwards through the time series) to eliminate phase shift. Filter frequency limits are 100-250 mHz, 250-500 mHz, and 500-1000 mHz. The effect of the anti-alias filter used to decimate data to 25 samples/s is seen at 12.5 Hz.

Figure 19. Histograms of End-Corner difference ratios for Livingston r.m.s. vertical component of ambient ground motion.

Figure 20. Histograms of End-Corner difference ratios for Livingston r.m.s. north component of ambient ground motion.

Figure 21. Histograms of End-Corner difference ratios for Livingston r.m.s. east component of ambient ground motion.

Figure 22. Histograms of End-Corner difference ratios for Hanford r.m.s. vertical component of ambient ground motion.

Figure 23. Histograms of End-Corner difference ratios for Hanford r.m.s. north component of ambient ground motion.

Figure 24. Histograms of End-Corner difference ratios for Hanford r.m.s. east component of ambient ground motion.

Figure 25. Cumulative distribution of independent and differential r.m.s. vertical-component displacements at Livingston South Arm.

Figure 26. Cumulative distribution of independent and differential r.m.s. vertical-component displacements at Livingston West Arm.

Figure 27. Cumulative distribution of independent and differential r.m.s. north-component displacements at Livingston South Arm.

Figure 28. Cumulative distribution of independent and differential r.m.s. north-component displacements at Livingston West Arm.

Figure 29. Cumulative distribution of independent and differential r.m.s. east-component displacements at Livingston South Arm.

Figure 30. Cumulative distribution of independent and differential r.m.s. east-component displacements at Livingston West Arm.

Figure 31. Cumulative distribution of independent and differential r.m.s. vertical-component displacements at Hanford Northwest Arm.

Figure 32. Cumulative distribution of independent and differential r.m.s. vertical-component displacements at Hanford Southwest Arm.

Figure 33. Cumulative distribution of independent and differential r.m.s. north-component displacements at Hanford Northwest Arm.

Figure 34. Cumulative distribution of independent and differential r.m.s. north-component displacements at Hanford Southwest Arm.

Figure 35. Cumulative distribution of independent and differential r.m.s. east-component displacements at Hanford Northwest Arm.

Figure 36. Cumulative distribution of independent and differential r.m.s. east-component displacements at Hanford Southwest Arm.

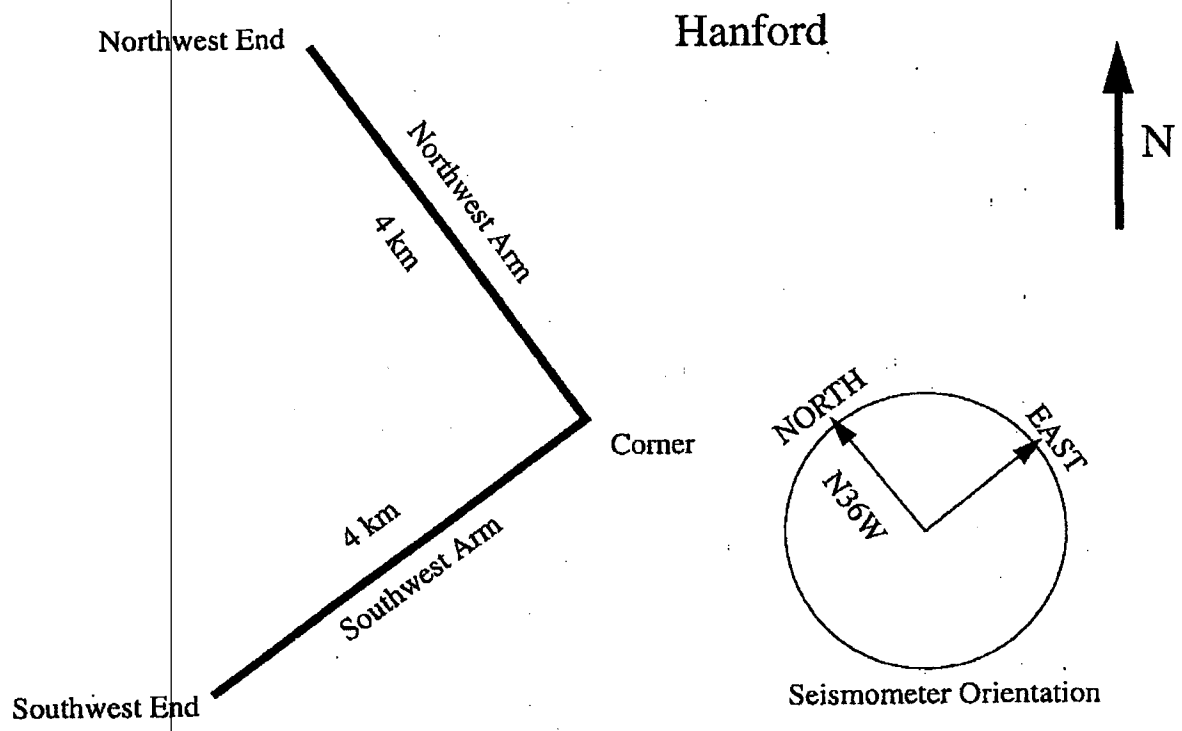
Hanford
Northwest End
Northwest Arm
4 km
Corner
4 km
Southwest Arm
Southwest End
N
NORTH
EAST
N36W
Seismometer Orientation

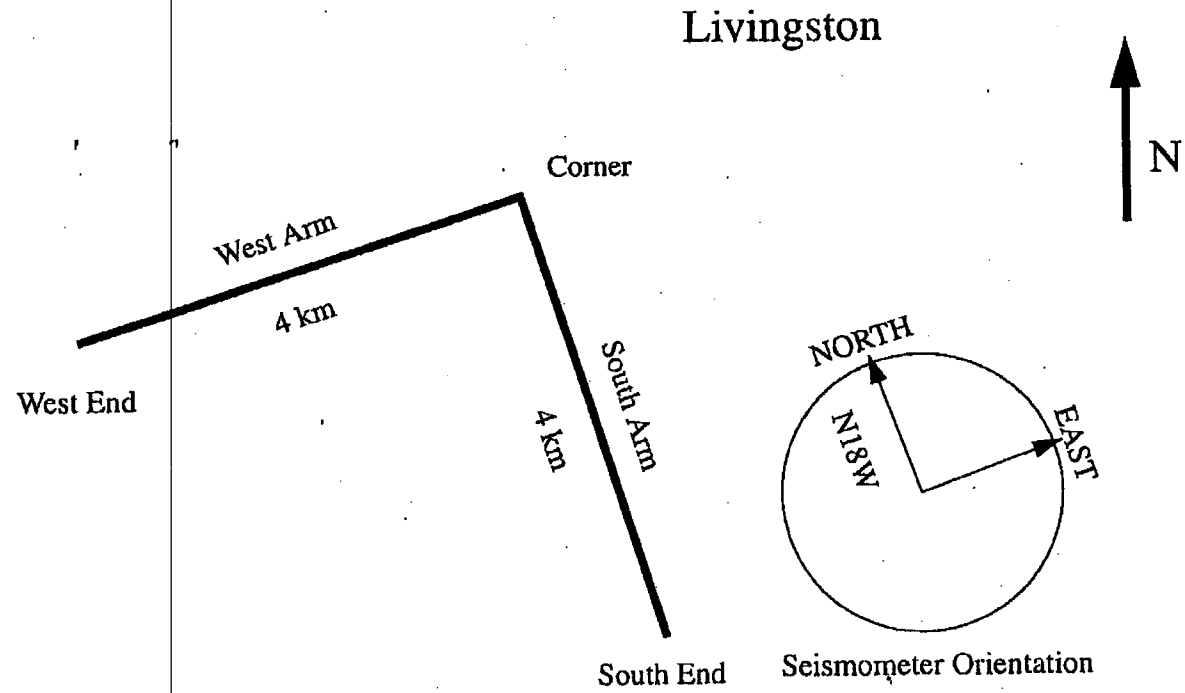
Livingston
Corner
West Arm
4 km
West End
South Arm
4 km
South End
N
NORTH
EAST
N18W
Seismometer Orientation

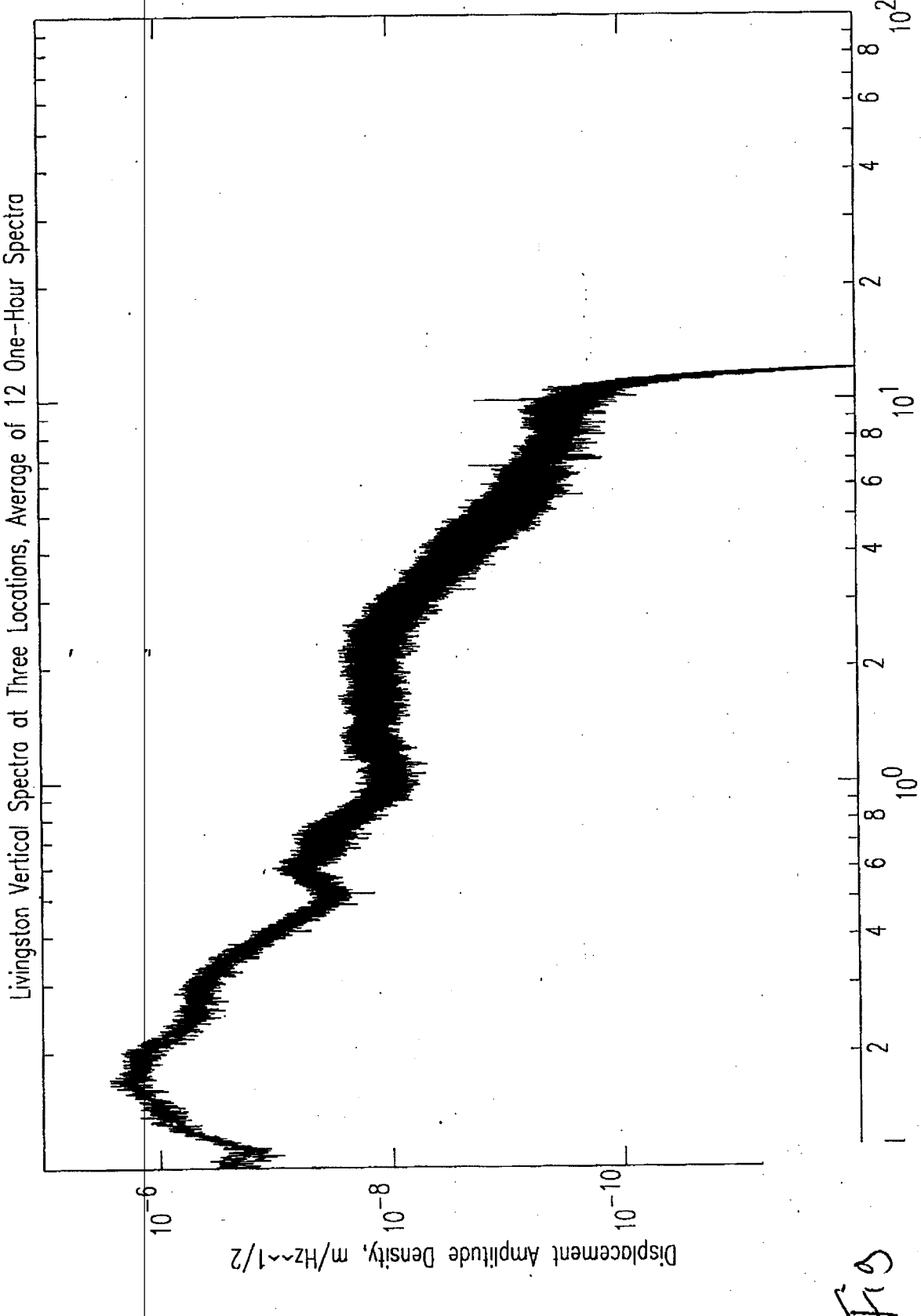
Livingston Vertical Spectra at Three Locations, Average of 12 One-Hour Spectra
Displacement Amplitude Density, m/Hz^^1/2
10^{-6}
10^{-8}
10^{-10}
1
2
4
6
8
10^{0}
2
4
6
8
10^{1}
2
4
6
8
10^{2}
Frequency, Hz

Fig 2

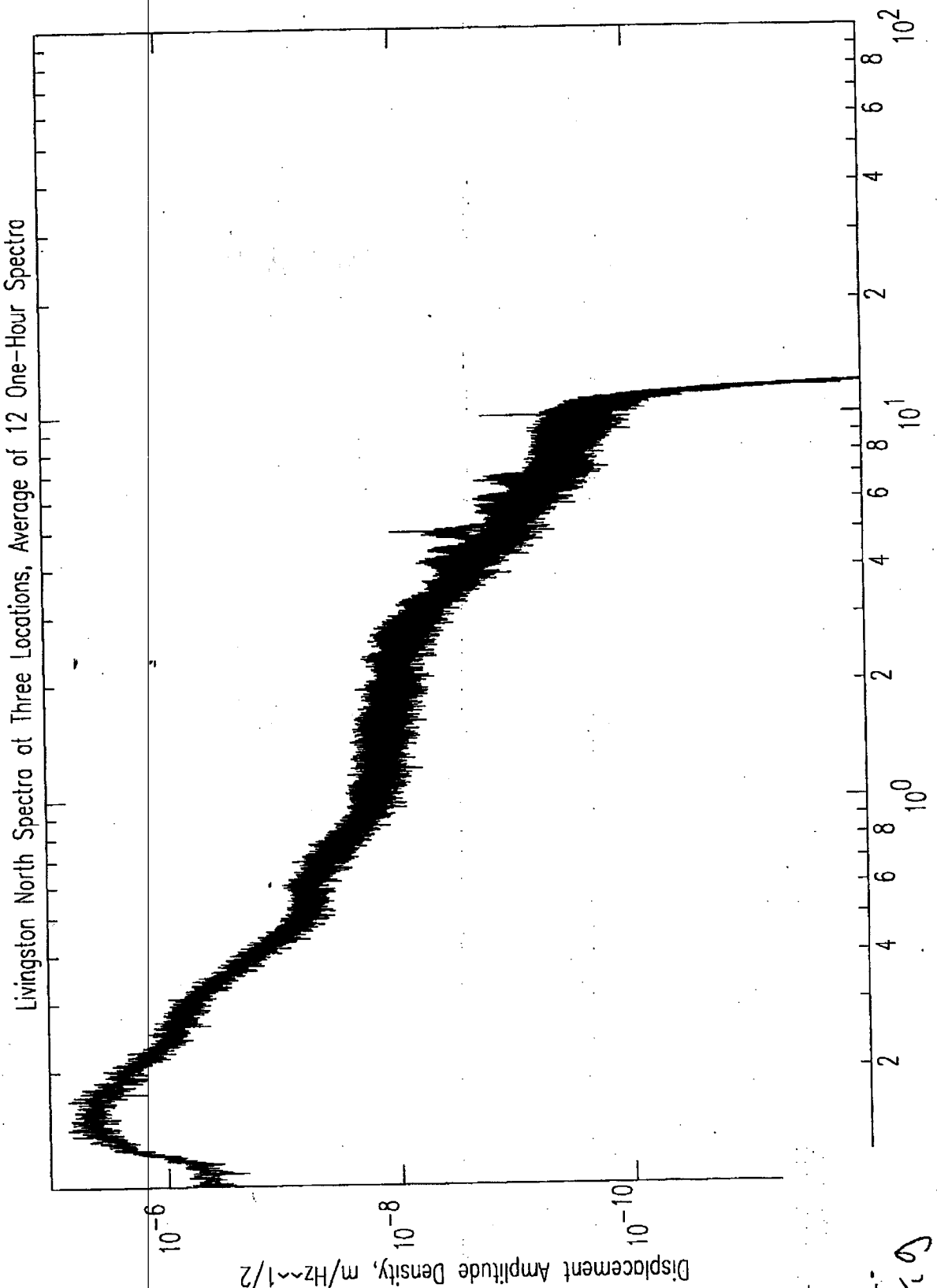
Livingston North Spectra at Three Locations, Average of 12 One-Hour Spectra
Displacement Amplitude Density, m/Hz^^1/2
10^{-6}
10^{-8}
10^{-10}
Frequency, Hz
2
4
6
8
10^{0}
2
4
6
8
10^{1}
2
4
6
8
10^{2}

Fig 3

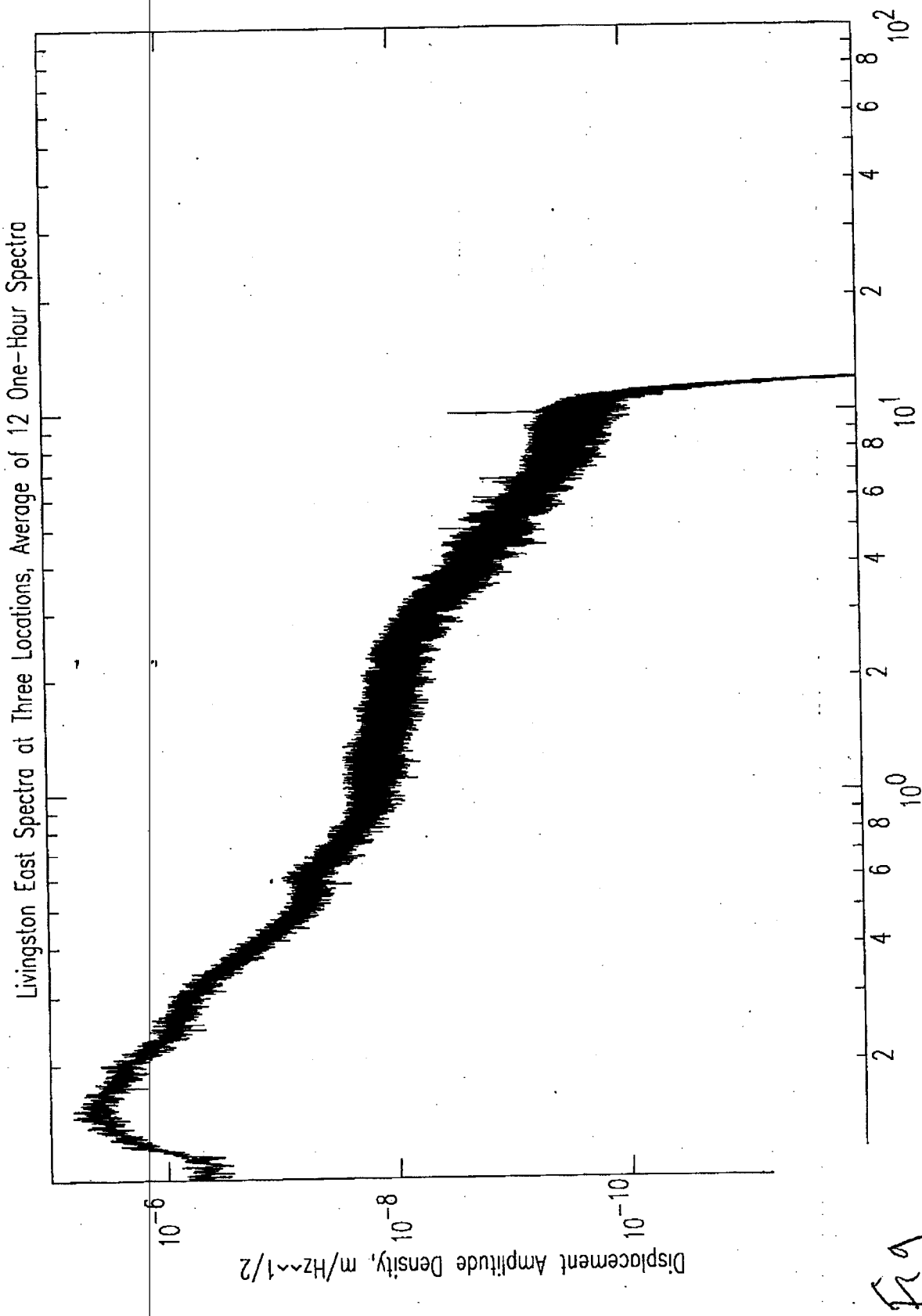
Livingston East Spectra at Three Locations, Average of 12 One-Hour Spectra
Displacement Amplitude Density, m/Hz^^1/2
10^{-6}
10^{-8}
10^{-10}
2
4
6
8
10^{0}
2
4
6
8
10^{1}
2
4
6
8
10^{2}
Frequency, Hz

Fig 4

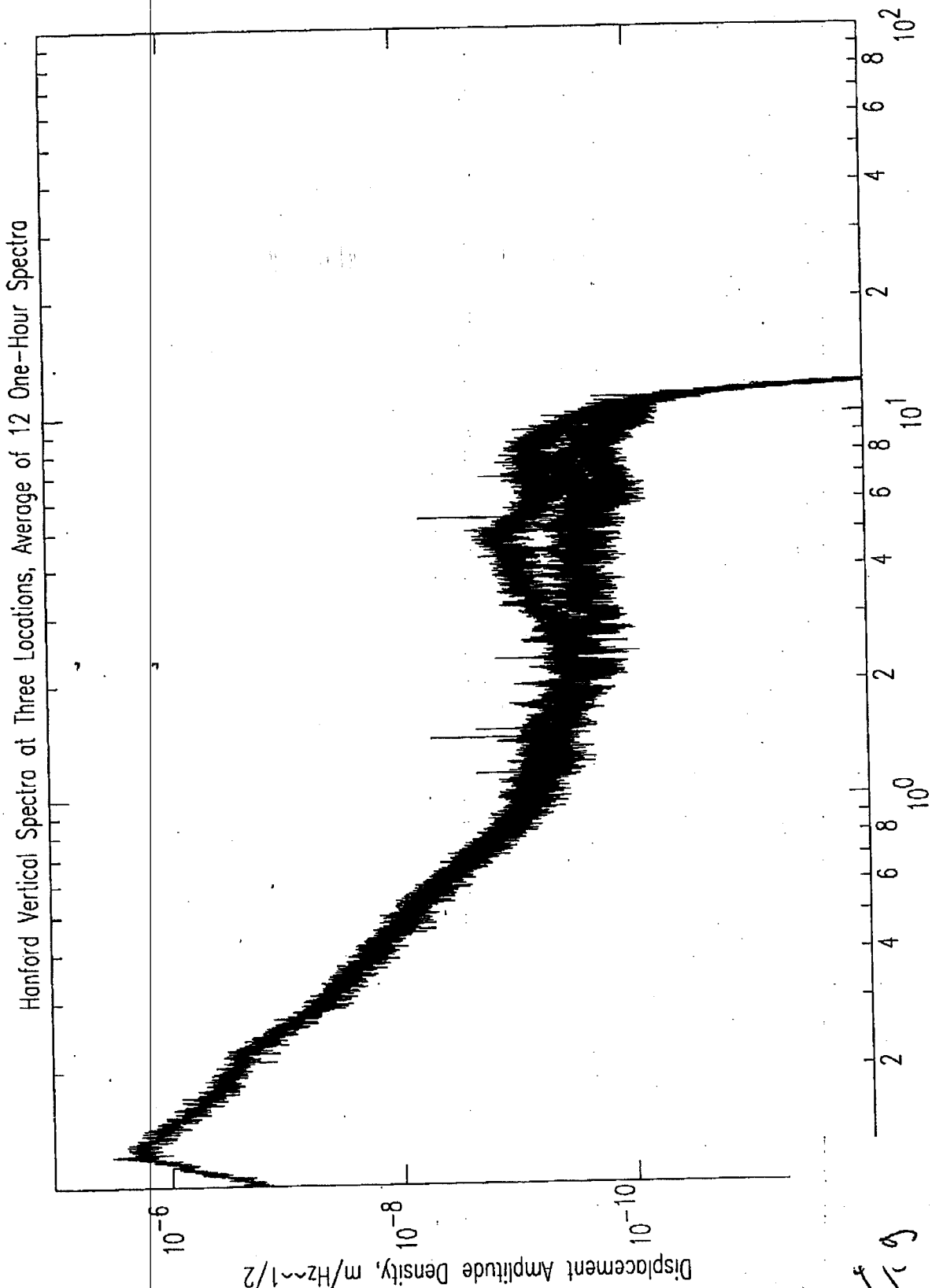
Hanford Vertical Spectra at Three Locations, Average of 12 One-Hour Spectra
Displacement Amplitude Density, m/Hz^^1/2
10^{-6}
10^{-8}
10^{-10}
Frequency, Hz
2
4
6
8
10^{0}
2
4
6
8
10^{1}
2
4
6
8
10^{2}

Fig 1

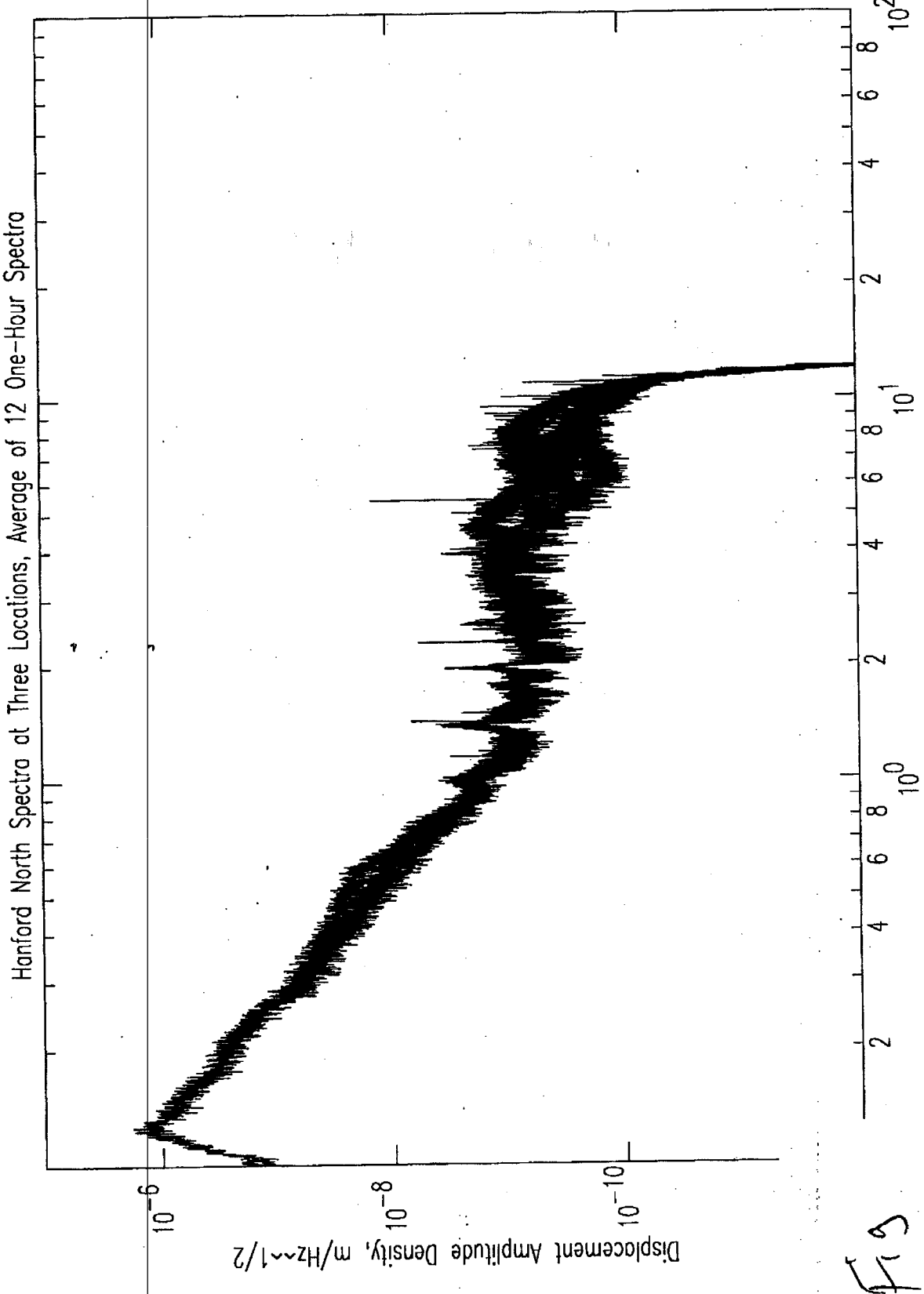
Hanford North Spectra at Three Locations, Average of 12 One-Hour Spectra
Displacement Amplitude Density, m/Hz^^1/2
Frequency, Hz
10^{-6}
10^{-8}
10^{-10}
10^{0}
10^{1}
10^{2}
2
4
6
8

Fig 6

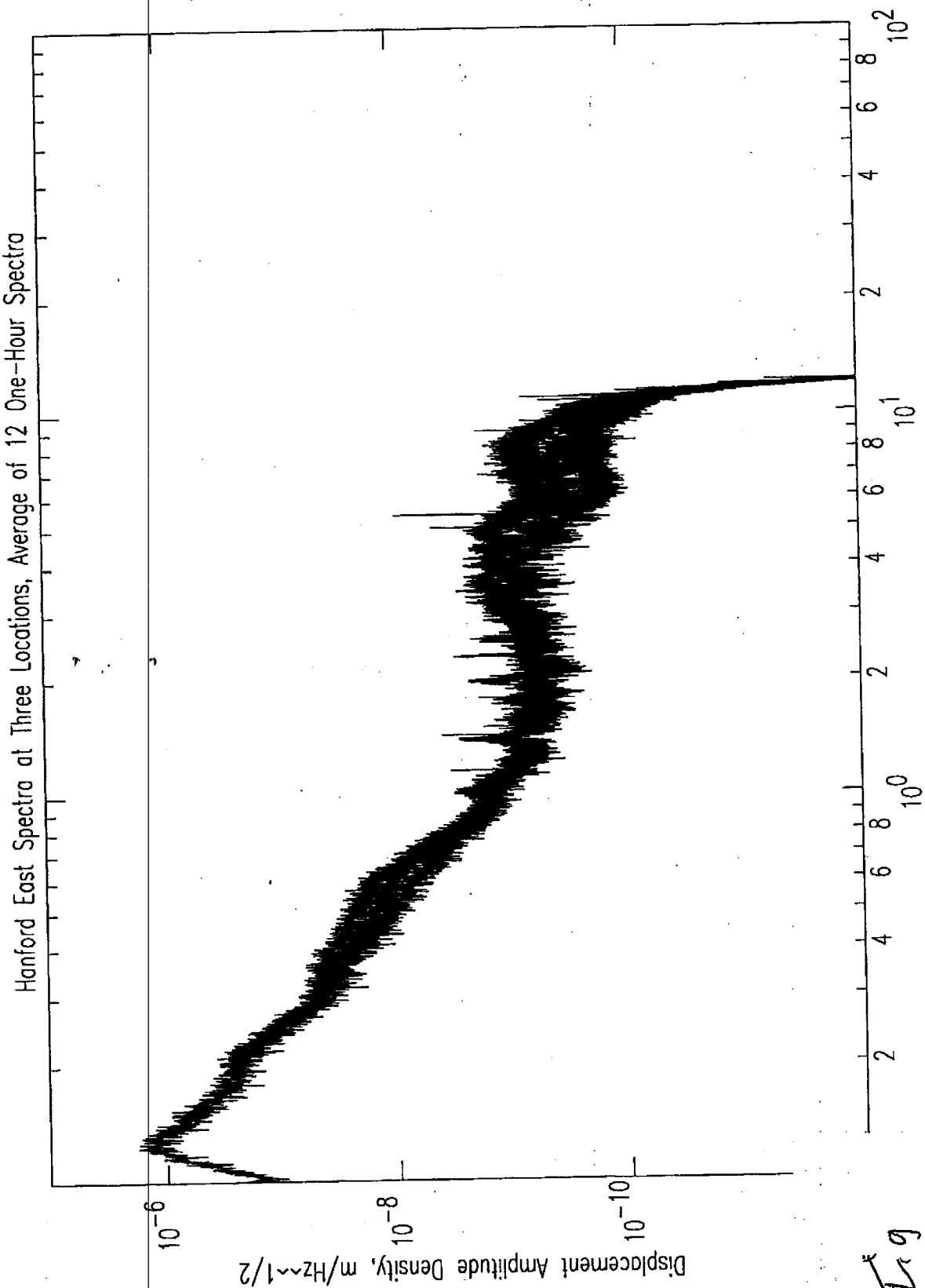
Hanford East Spectra at Three Locations, Average of 12 One-Hour Spectra
Displacement Amplitude Density, m/Hz^^1/2
10^{-6}
10^{-8}
10^{-10}
2
4
6
8
10^{0}
2
4
6
8
10^{1}
2
4
6
8
10^{2}
Frequency, Hz

Fig 7

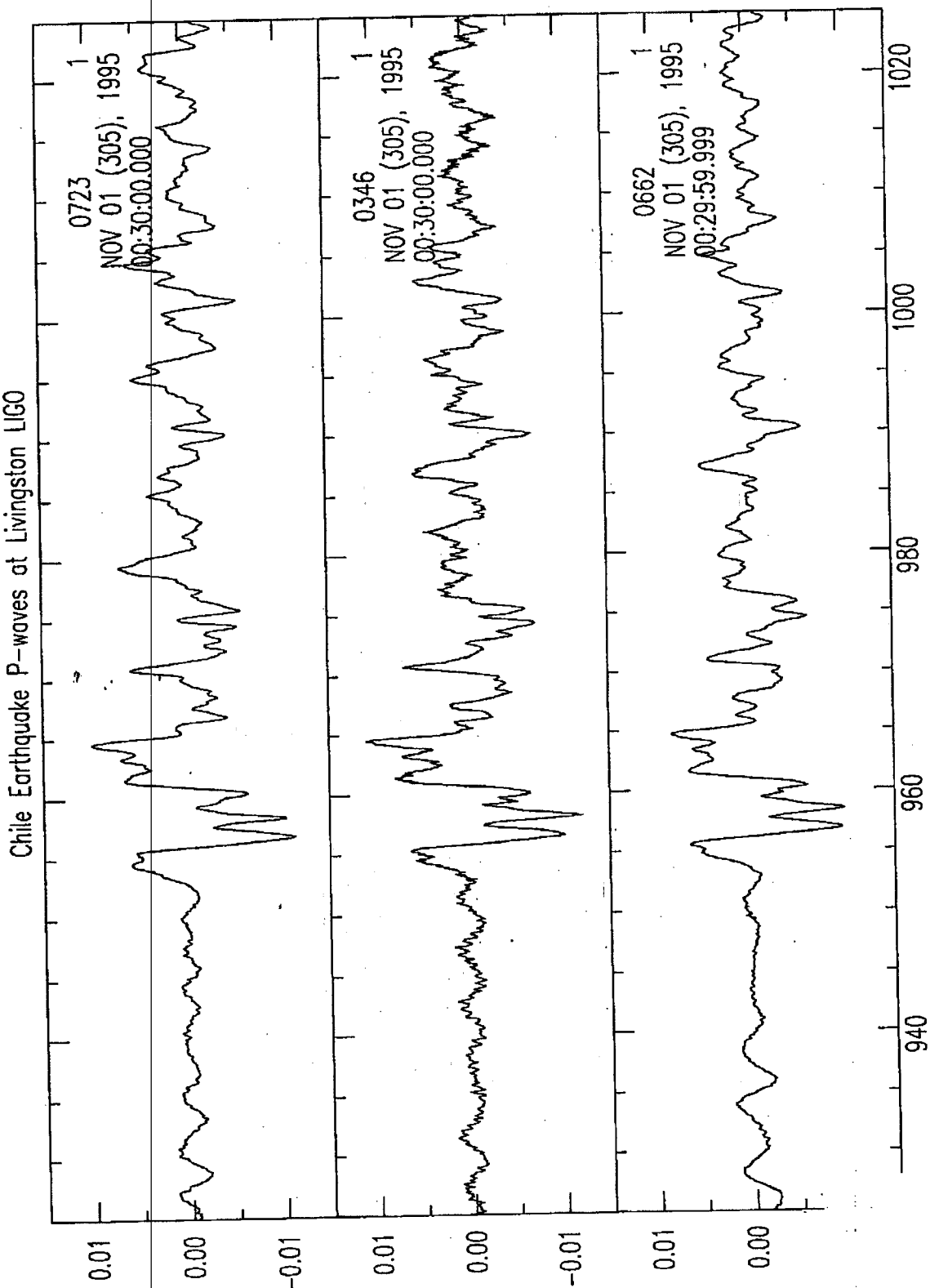
Chile Earthquake P-waves at Livingston LIGO
0723
NOV 01 (305), 1995
00:30:00.000
0346
NOV 01 (305), 1995
00:30:00.000
0662
NOV 01 (305), 1995
00:29:59.999
0.01
0.00
-0.01
940
960
980
1000
1020

Fig 6

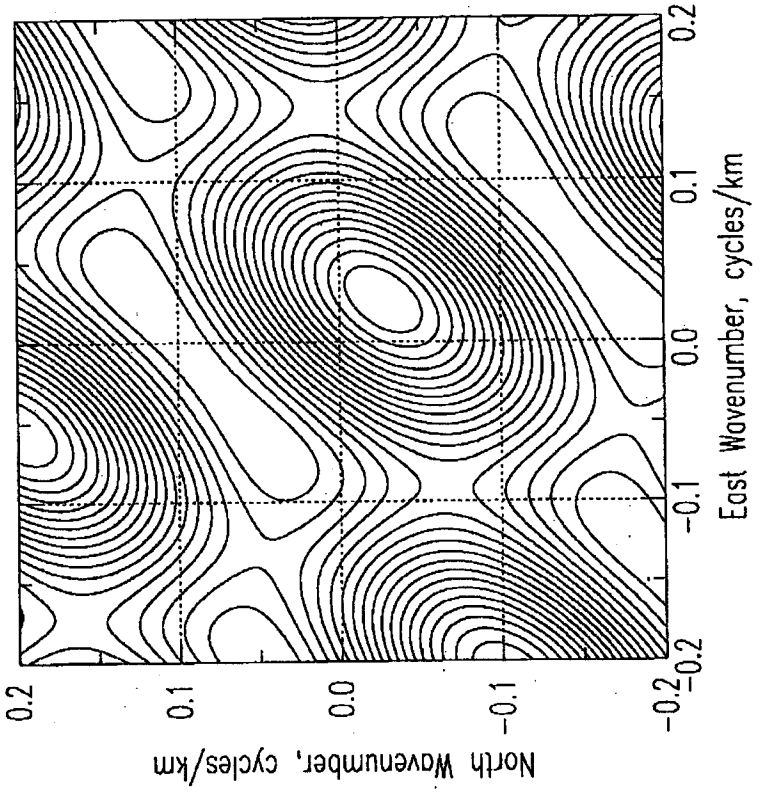
North Wavenumber, cycles/km
0.2
0.1
0.0
-0.1
-0.2
East Wavenumber, cycles/km
-0.2
-0.1
0.0
0.1
0.2

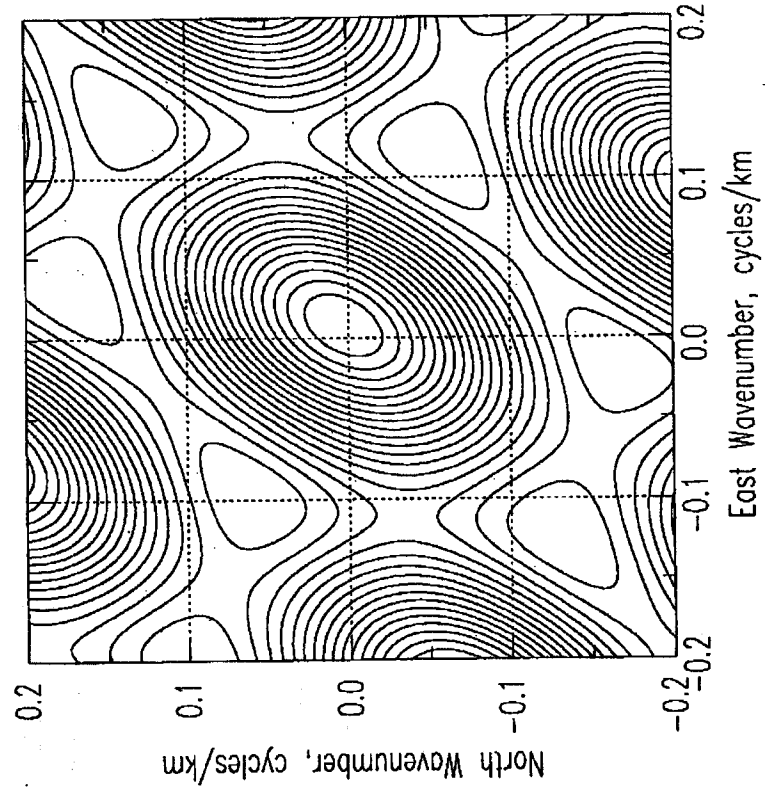
North Wavenumber, cycles/km
0.2
0.1
0.0
-0.1
-0.2
East Wavenumber, cycles/km
-0.2
-0.1
0.0
0.1
0.2

Fig 9

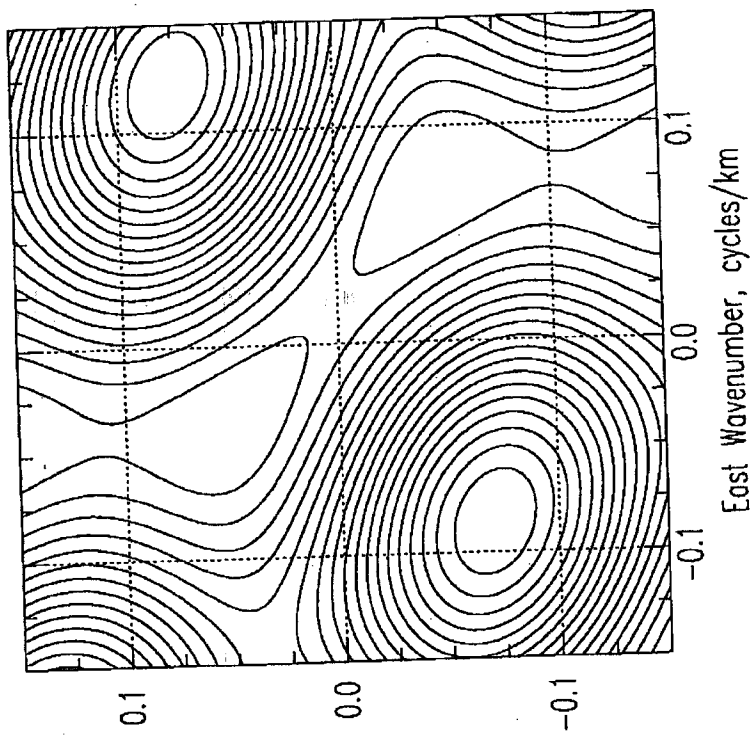
0.1
0.0
-0.1
North Wavenumber, cycles/km
0.1
0.0
-0.1
East Wavenumber, cycles/km

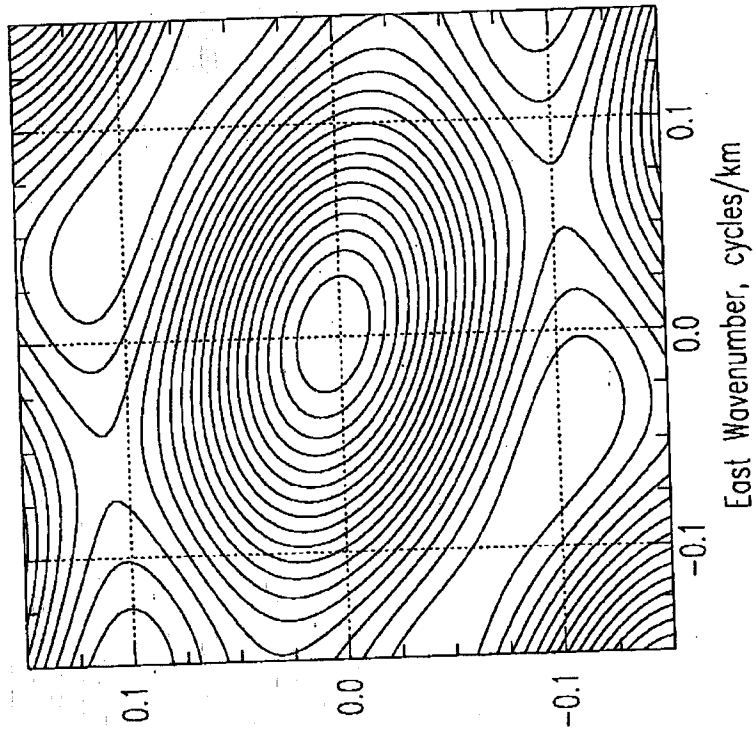
0.1
0.0
-0.1
North Wavenumber, cycles/km
0.1
0.0
-0.1
East Wavenumber, cycles/km

Fig 10

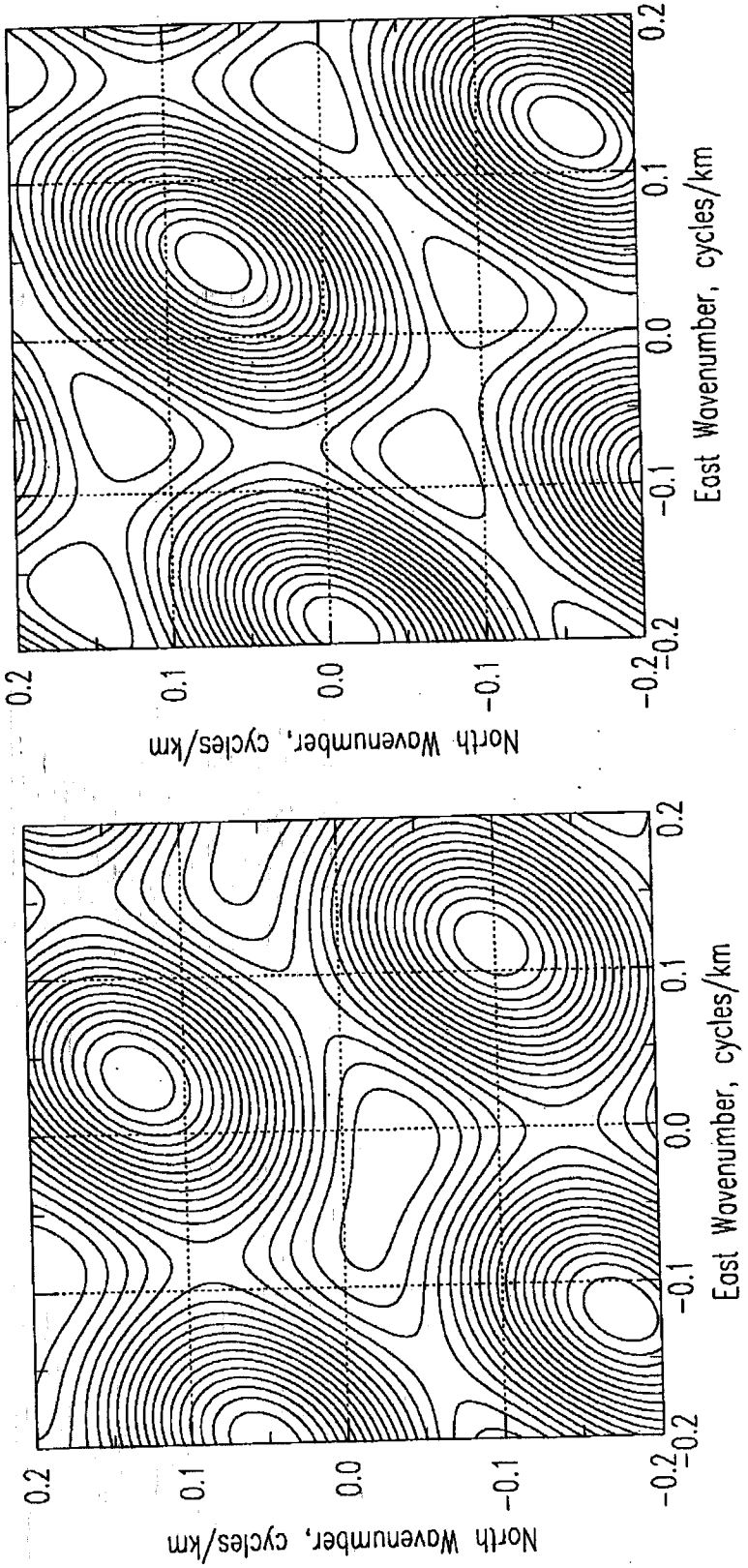
North Wavenumber, cycles/km
0.2
0.1
0.0
-0.1
-0.2
East Wavenumber, cycles/km
0.2
0.1
0.0
-0.1
-0.2
North Wavenumber, cycles/km
0.2
0.1
0.0
-0.1
-0.2
East Wavenumber, cycles/km
0.2
0.1
0.0
-0.1
-0.2

Figure 11

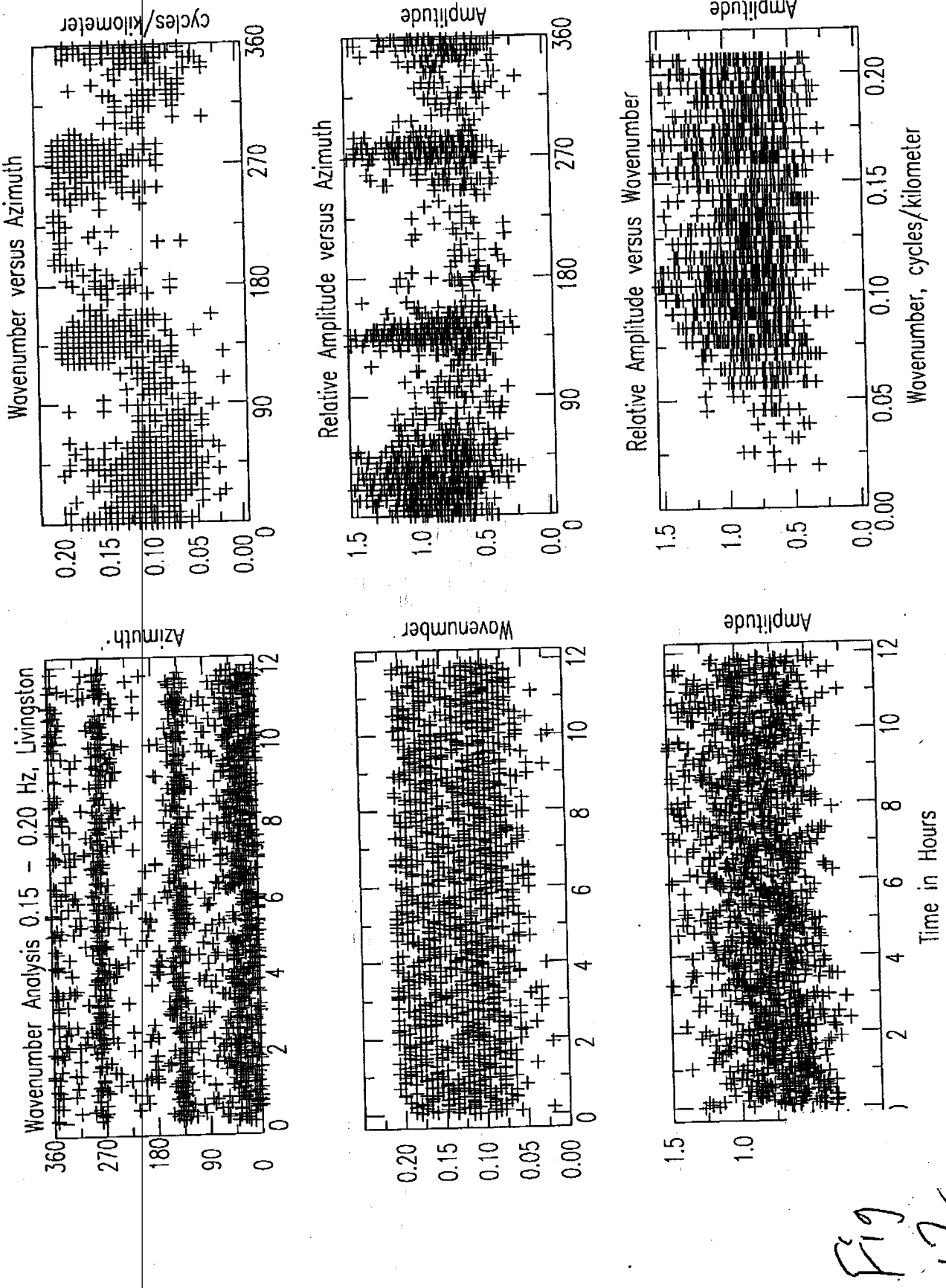
Wavenumber Analysis 0.15 - 0.20 Hz, Livingston
Azimuth
Wavenumber
Amplitude
Time in Hours
Wavenumber versus Azimuth
cycles/kilometer
Relative Amplitude versus Azimuth
Amplitude
Relative Amplitude versus Wavenumber
Amplitude
Wavenumber, cycles/kilometer

Fig 12

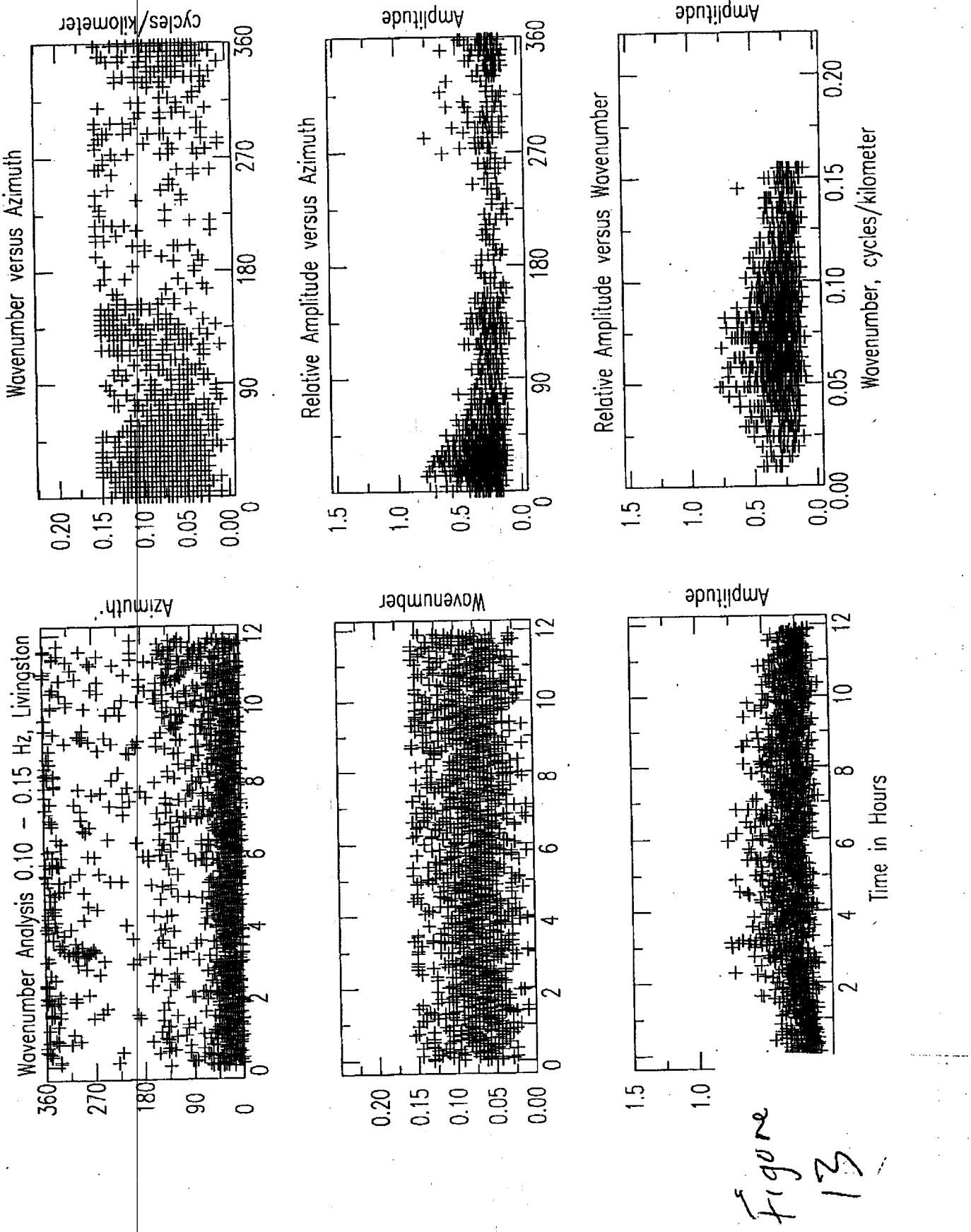
Wavenumber Analysis 0.10 - 0.15 Hz, Livingston
Azimuth
Wavenumber
Amplitude
Time in Hours
Wavenumber versus Azimuth
cycles/kilometer
Relative Amplitude versus Azimuth
Amplitude
Relative Amplitude versus Wavenumber
Amplitude
Wavenumber, cycles/kilometer

Figure 13

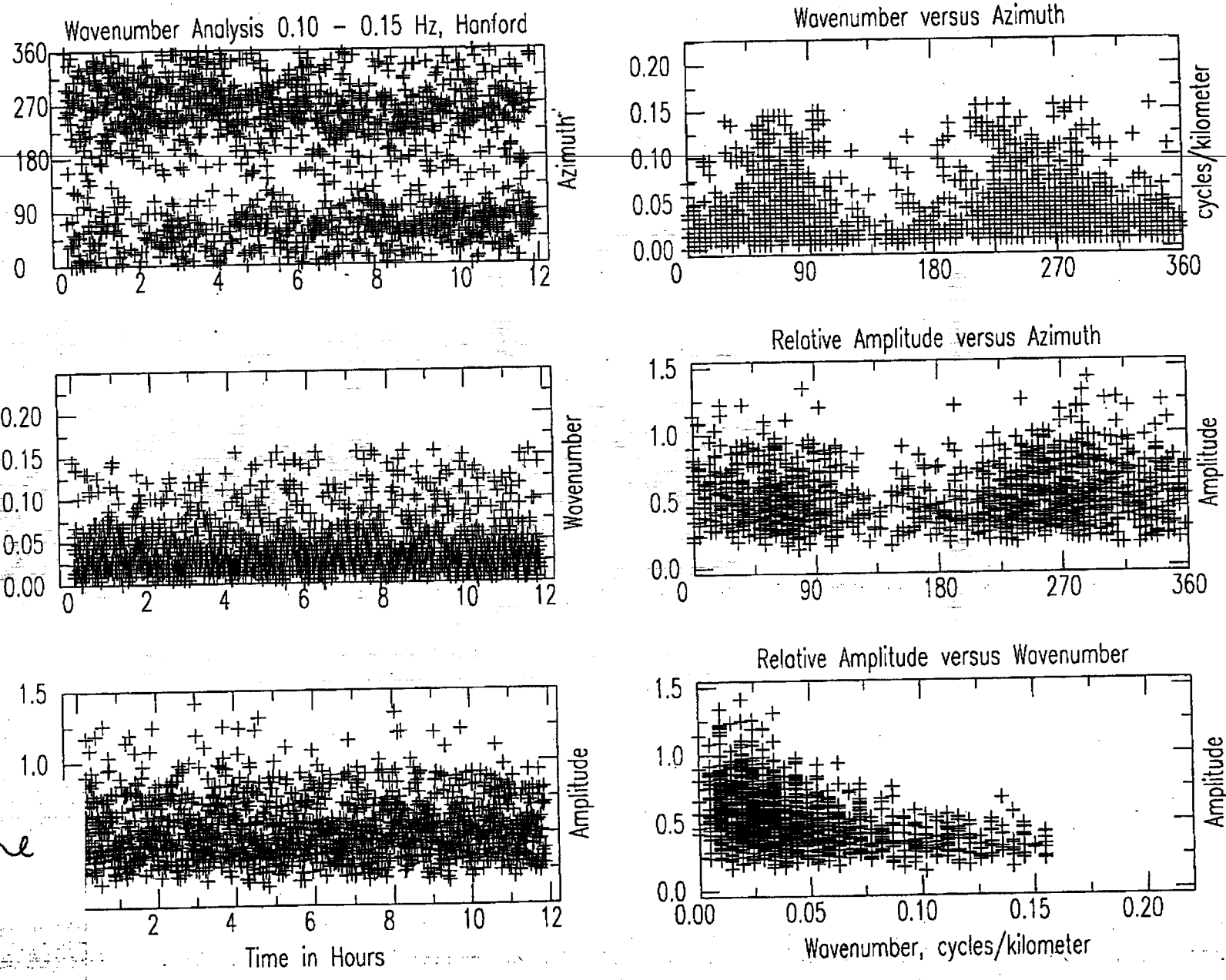

Figure 14

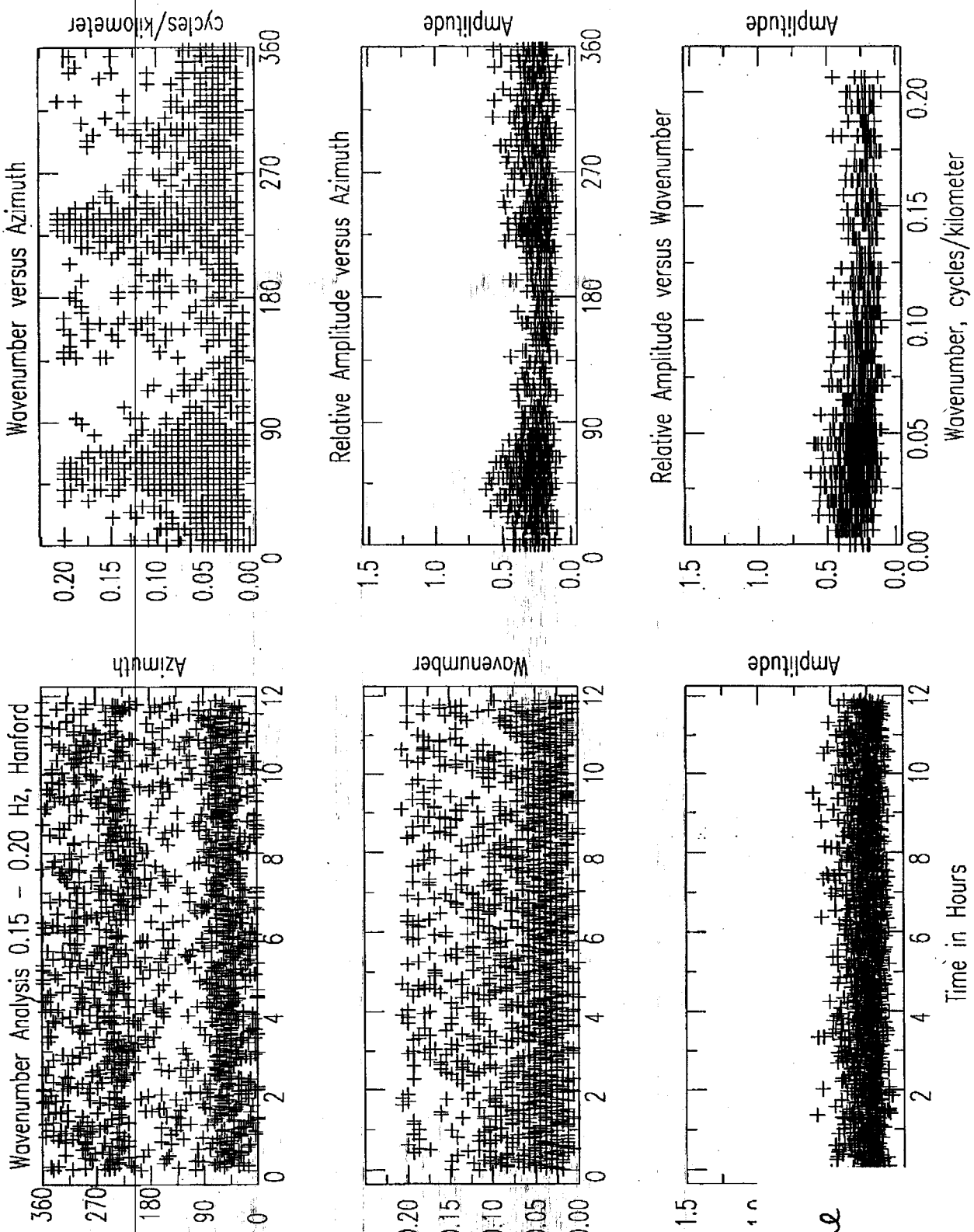
Wavenumber Analysis 0.15 - 0.20 Hz, Hanford
Azimuth
Wavenumber
Amplitude
Time in Hours
Wavenumber versus Azimuth
cycles/kilometer
Relative Amplitude versus Azimuth
Amplitude
Relative Amplitude versus Wavenumber
Amplitude
Wavenumber, cycles/kilometer

Figure 15

Hanford Azimuths and Wavenumbers

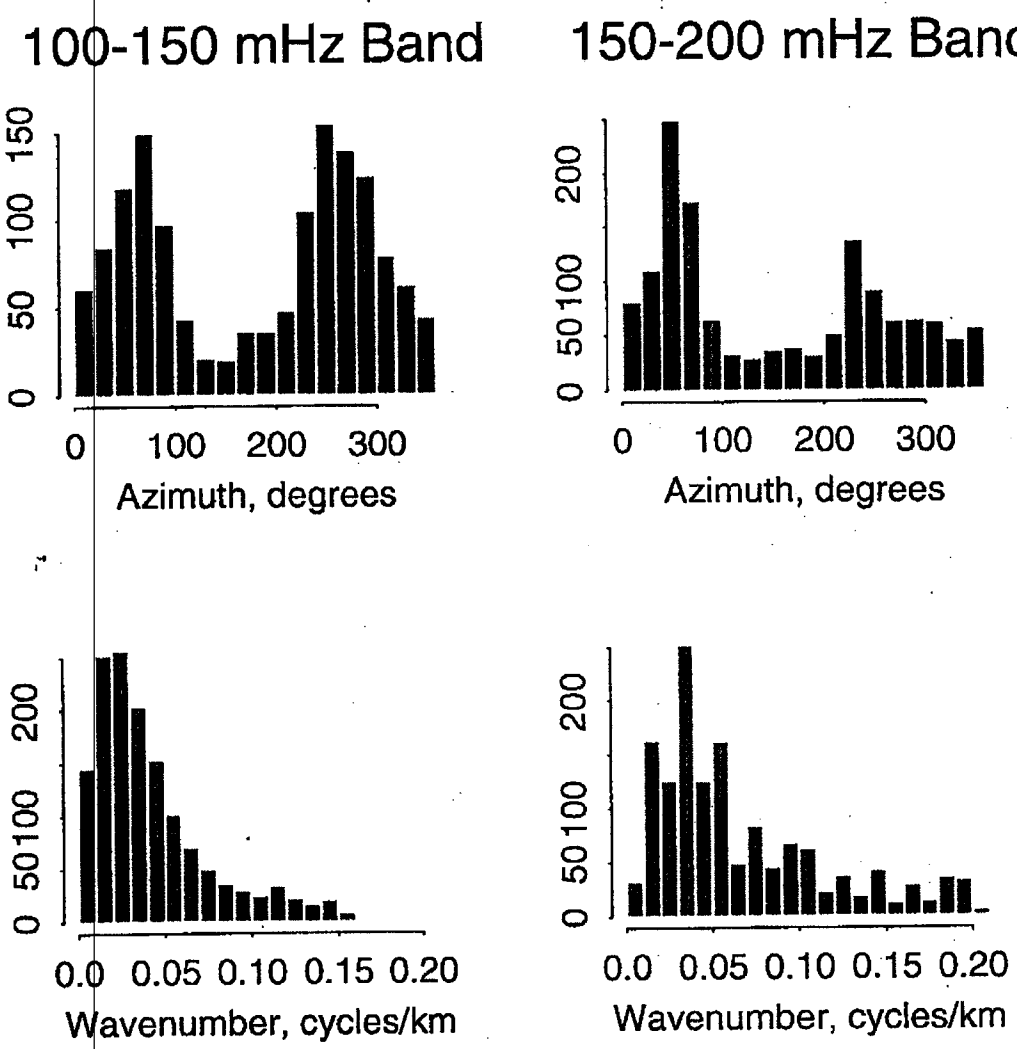

Fig 16

Livingston Azimuths and Wavenumbers

100-150 mHz Band

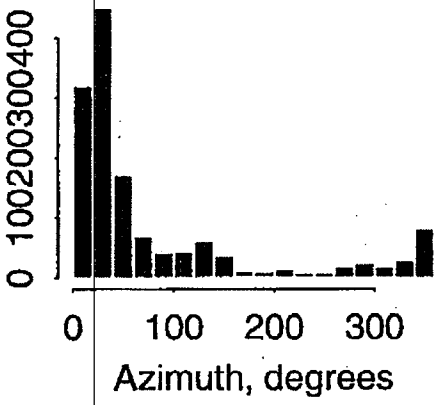

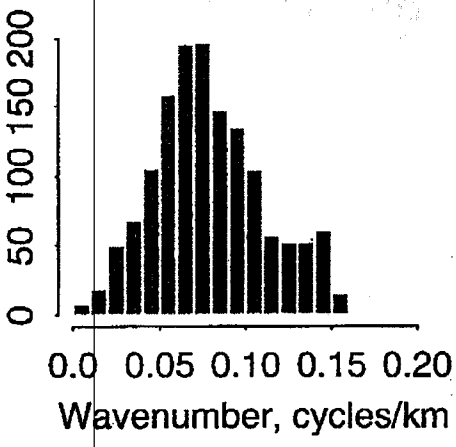

150-200 mHz Band

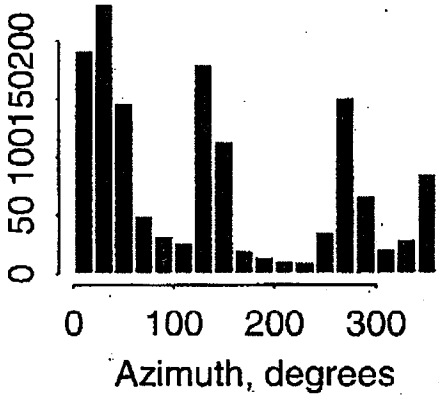

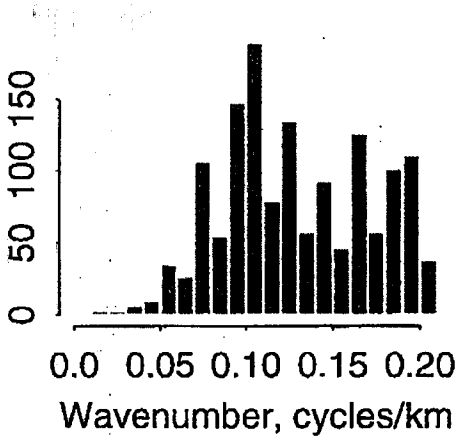

Fig 11

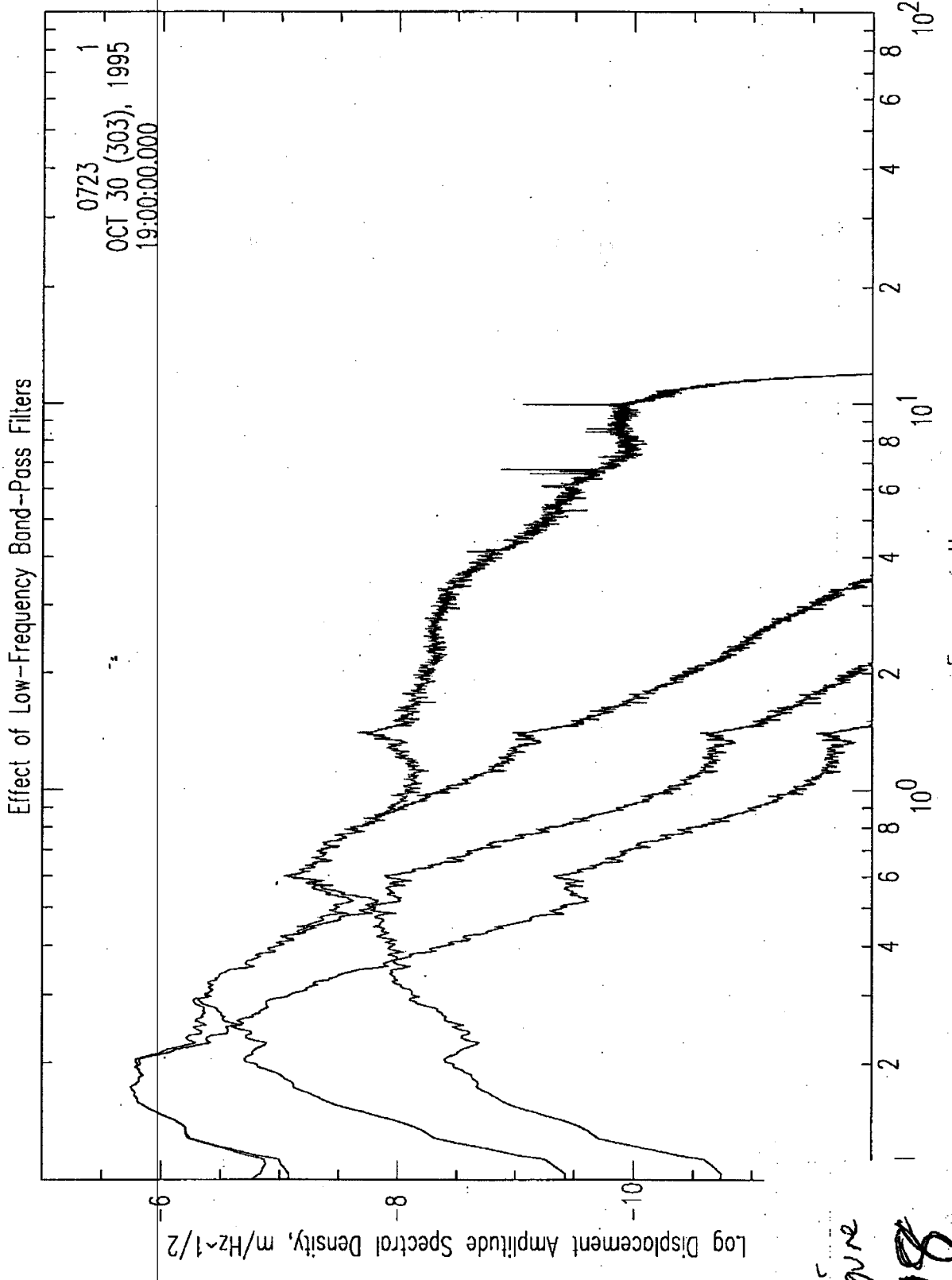
Effect of Low-Frequency Band-Pass Filters
0723
OCT 30 (303), 1995
19:00:00.000
1
Log Displacement Amplitude Spectral Density, m/Hz^1/2
-6
-8
-10
Frequency, Hz
1
2
4
6
8
10^0
2
4
6
8
10^1
2
4
6
8
10^2

Figure 18

Livingston Vertical Difference Ratios

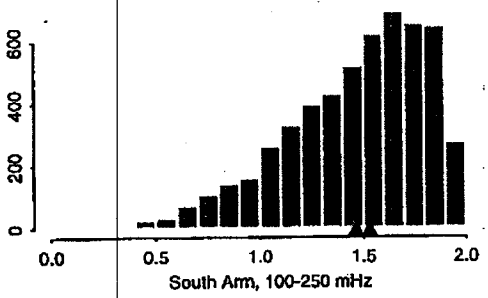

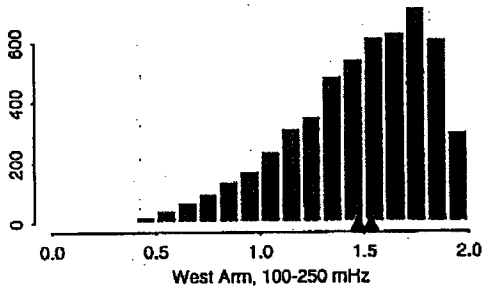

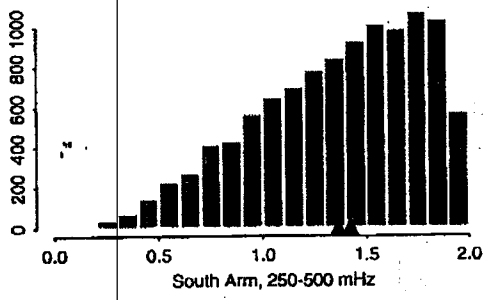

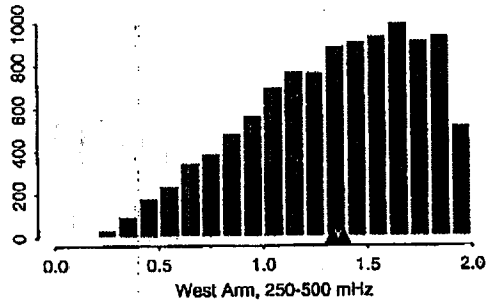

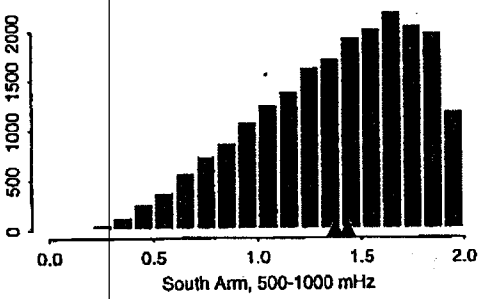

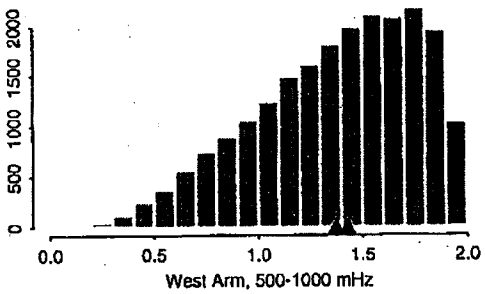

F9 19

Livingston North Difference Ratios

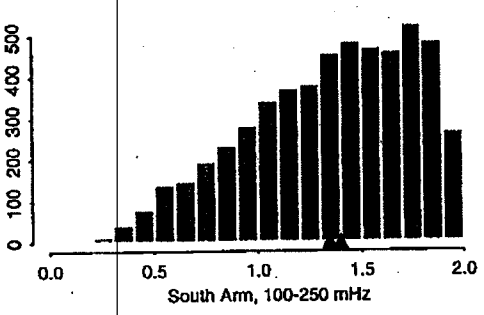

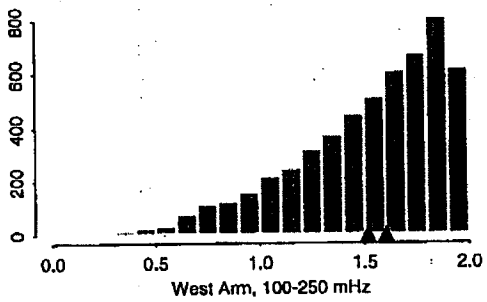

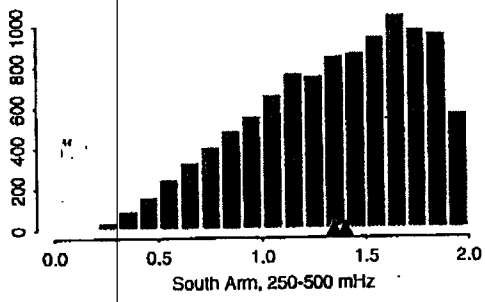

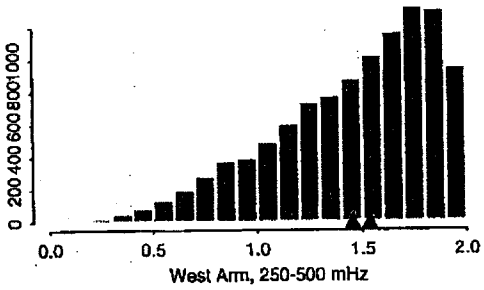

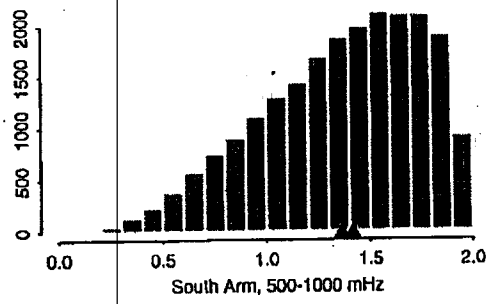

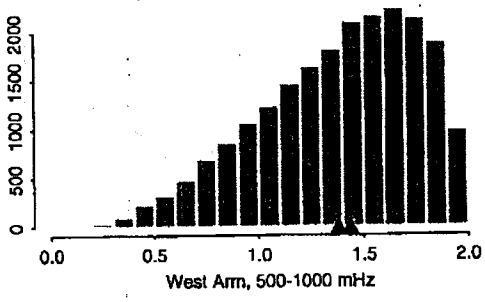

Fig 28

Livingston East Difference Ratios

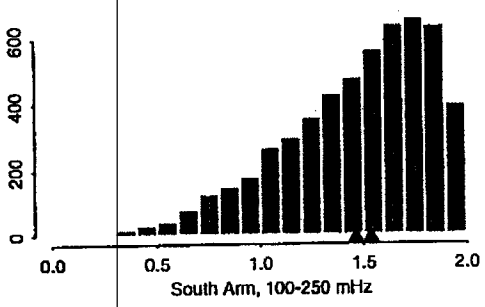

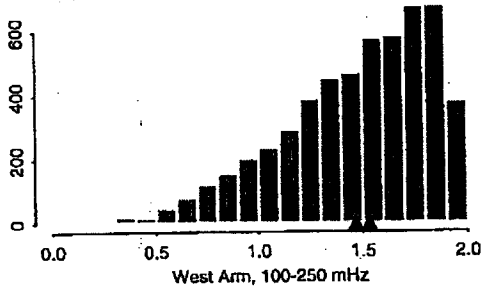

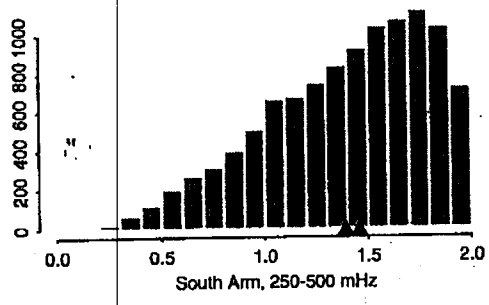

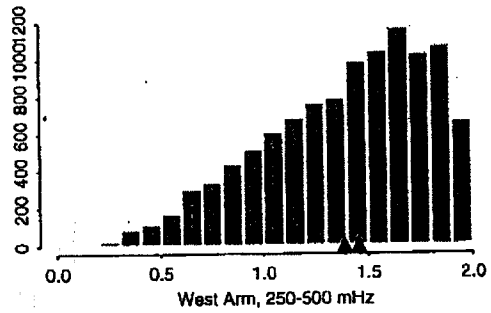

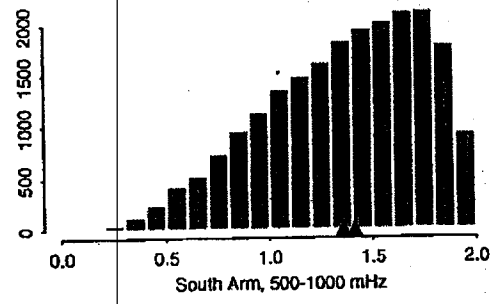

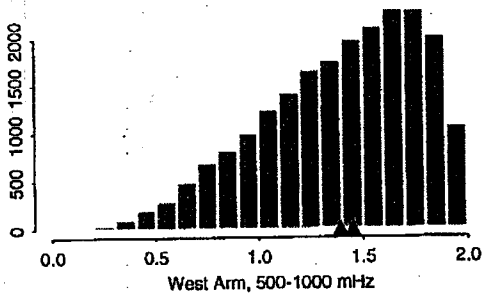

Fig 21

Hanford Vertical Difference Ratios

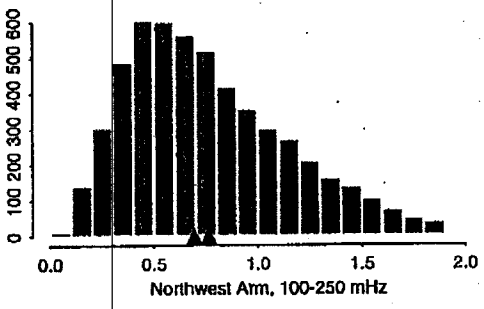

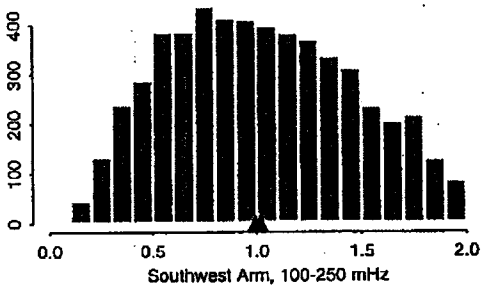

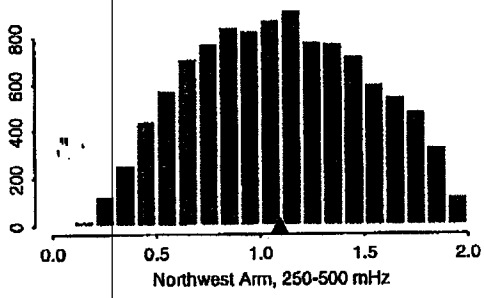

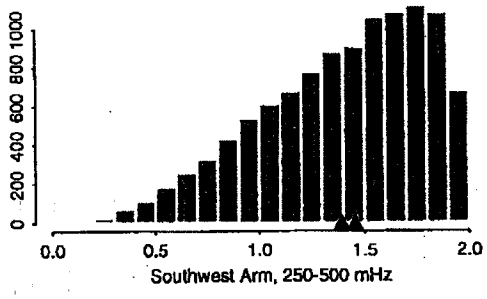

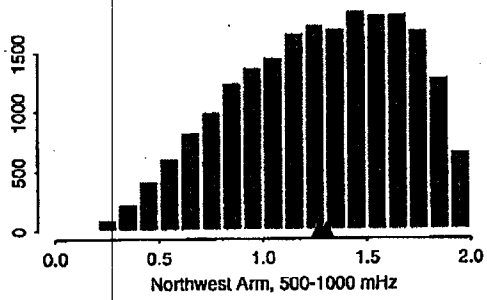

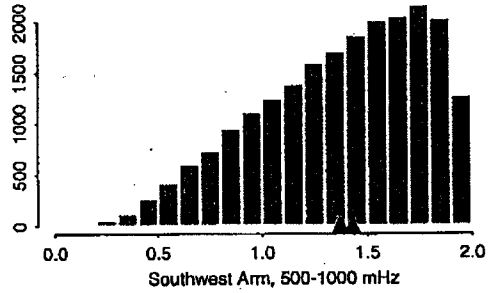

Fig 22

Hanford North Difference Ratios

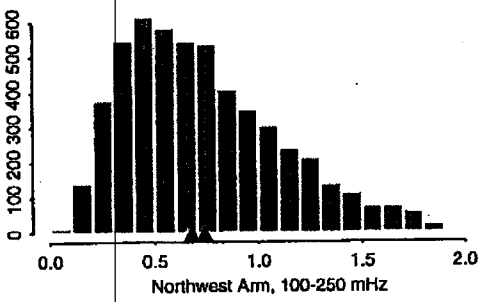

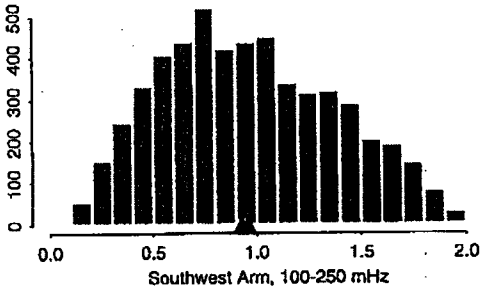

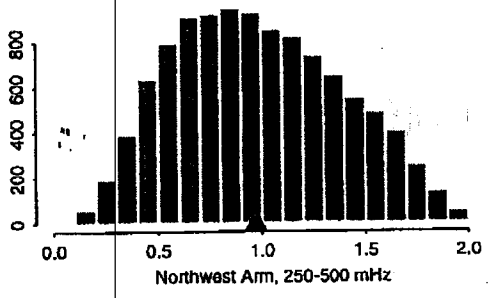

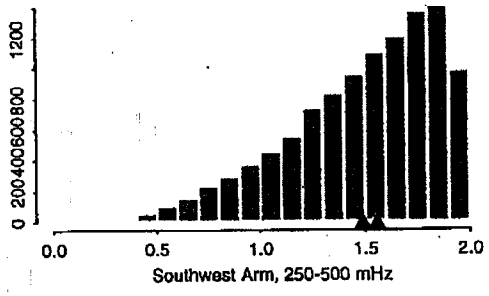

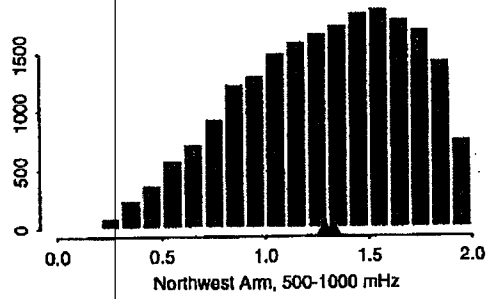

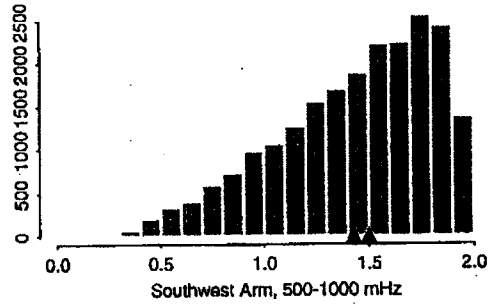

F9 23

Hanford East Difference Ratios

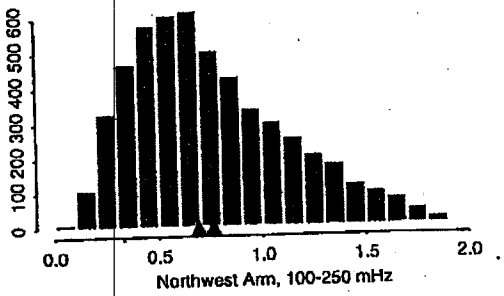

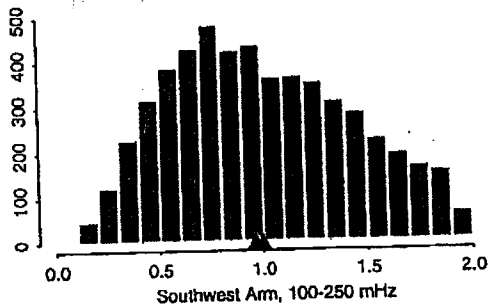

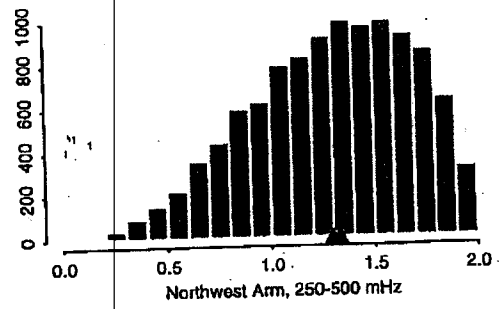

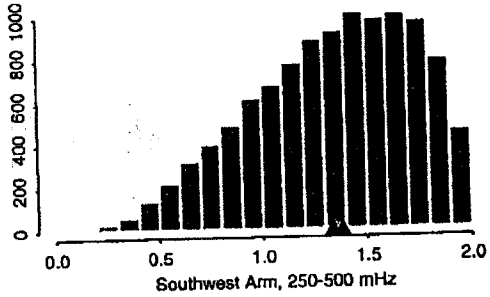

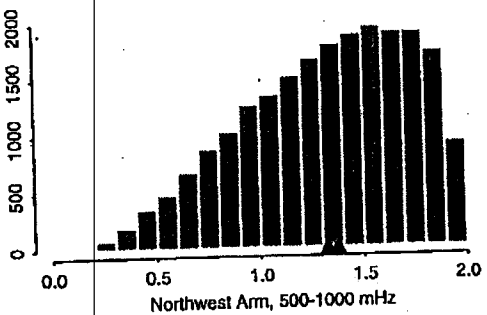

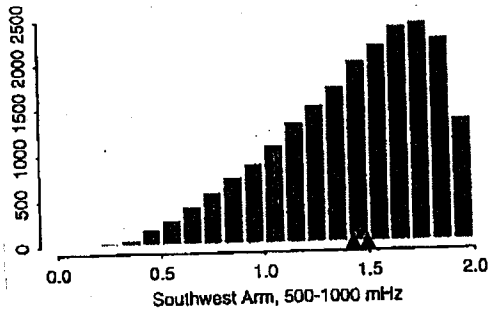

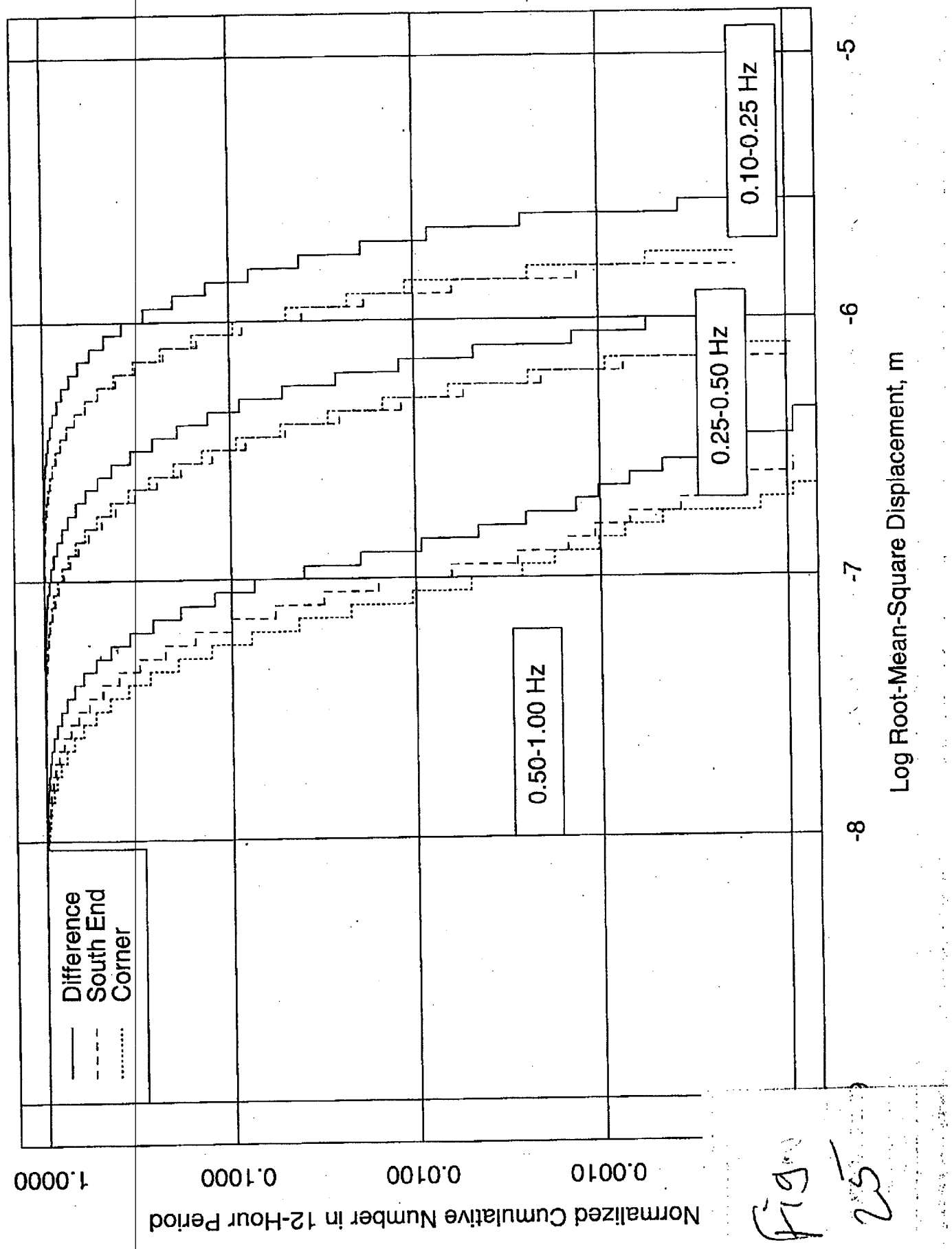
Livingston South Arm Vertical Difference
Difference
South End
Corner
0.10-0.25 Hz
0.25-0.50 Hz
0.50-1.00 Hz
Normalized Cumulative Number in 12-Hour Period
0.0010
0.0100
0.1000
1.0000
Log Root-Mean-Square Displacement, m
-5
-6
-7
-8

Fig 25

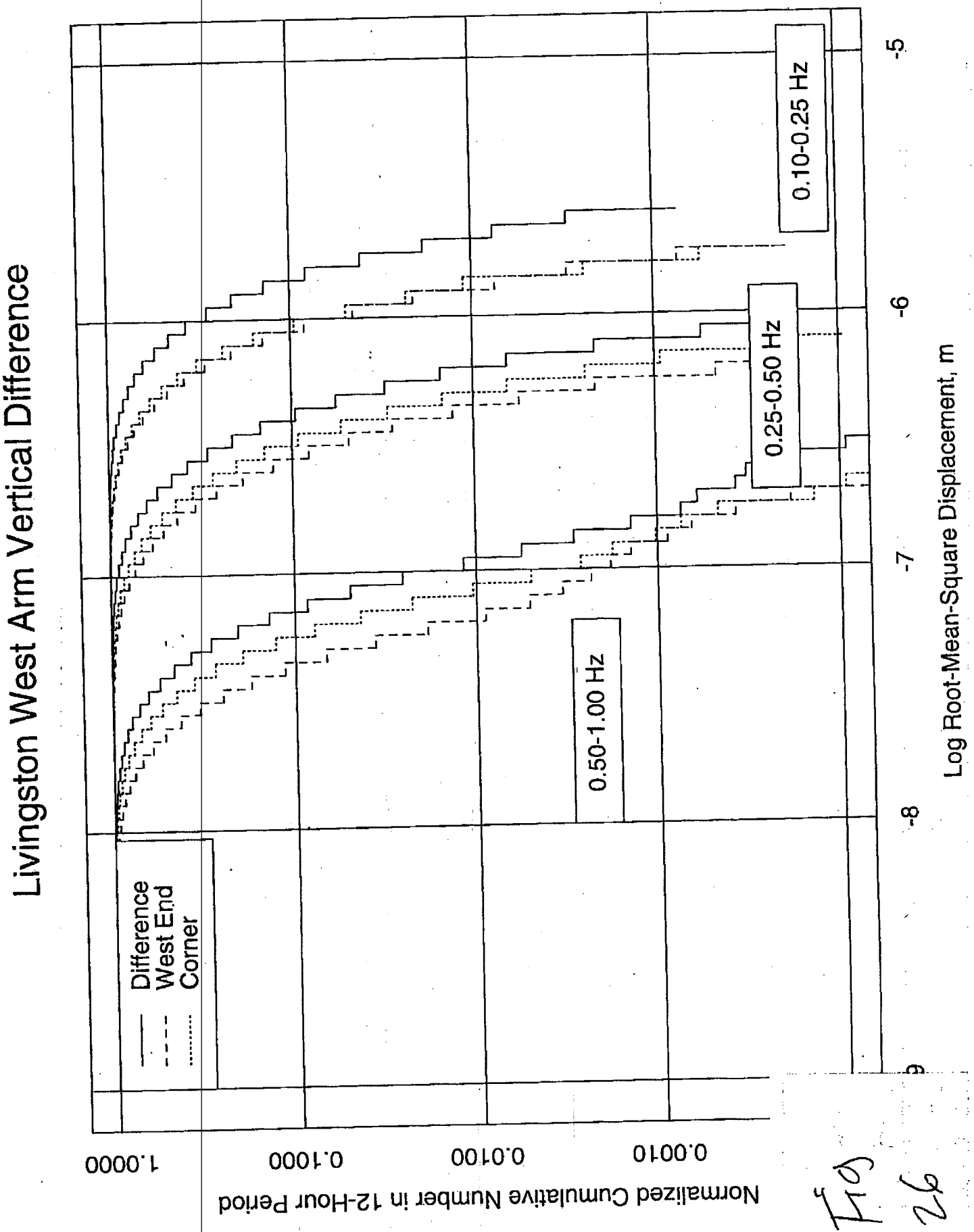
Livingston West Arm Vertical Difference
Difference
West End
Corner
0.10-0.25 Hz
0.25-0.50 Hz
0.50-1.00 Hz
Normalized Cumulative Number in 12-Hour Period
0.0010
0.0100
0.1000
1.0000
Log Root-Mean-Square Displacement, m
-5
-6
-7
-8

Fig 26

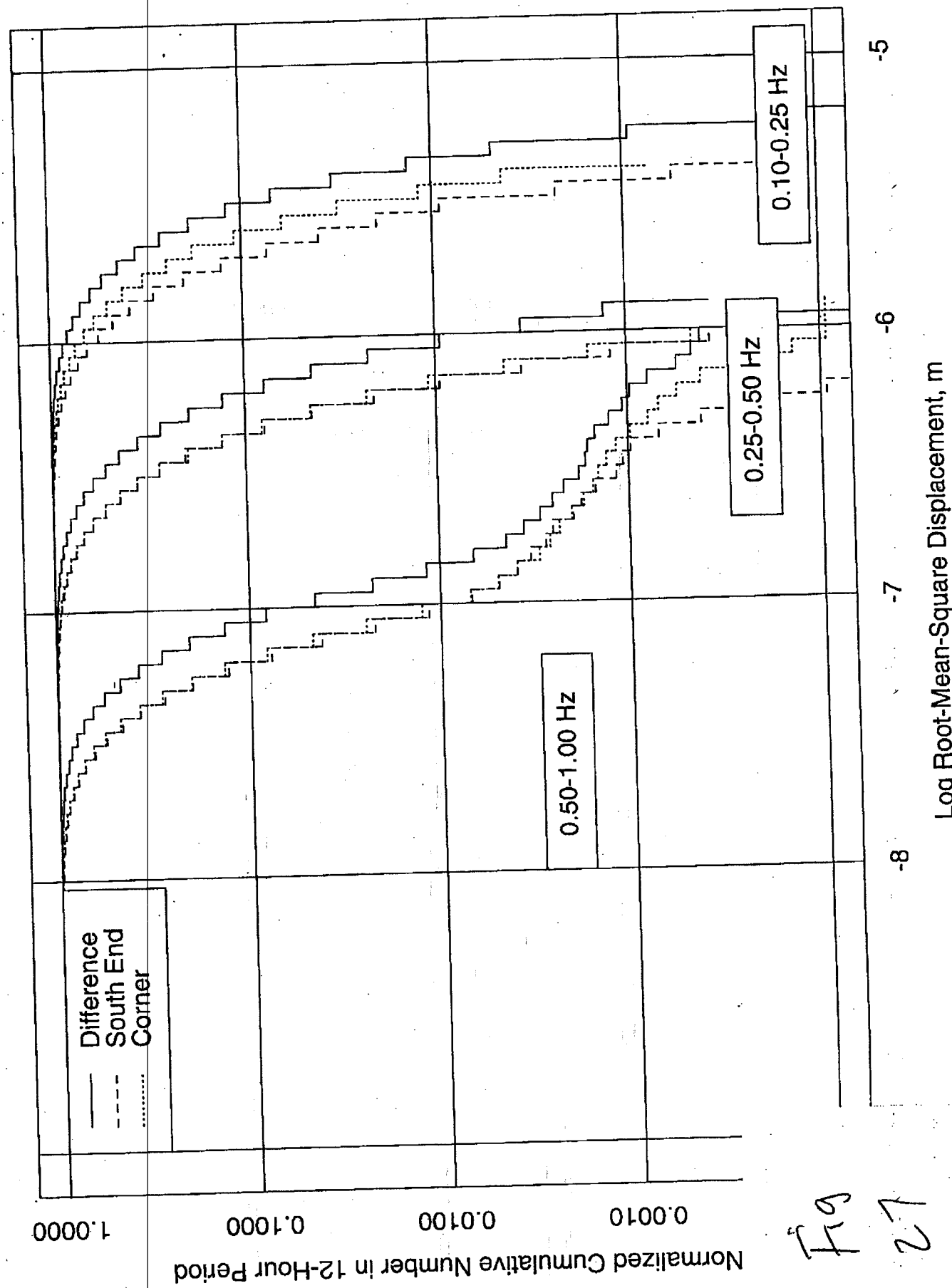
Livingston South Arm North Difference
Difference
South End
Corner
0.10-0.25 Hz
0.25-0.50 Hz
0.50-1.00 Hz
Normalized Cumulative Number in 12-Hour Period
0.0010
0.0100
0.1000
1.0000
Log Root-Mean-Square Displacement, m
-5
-6
-7
-8

Fig 21

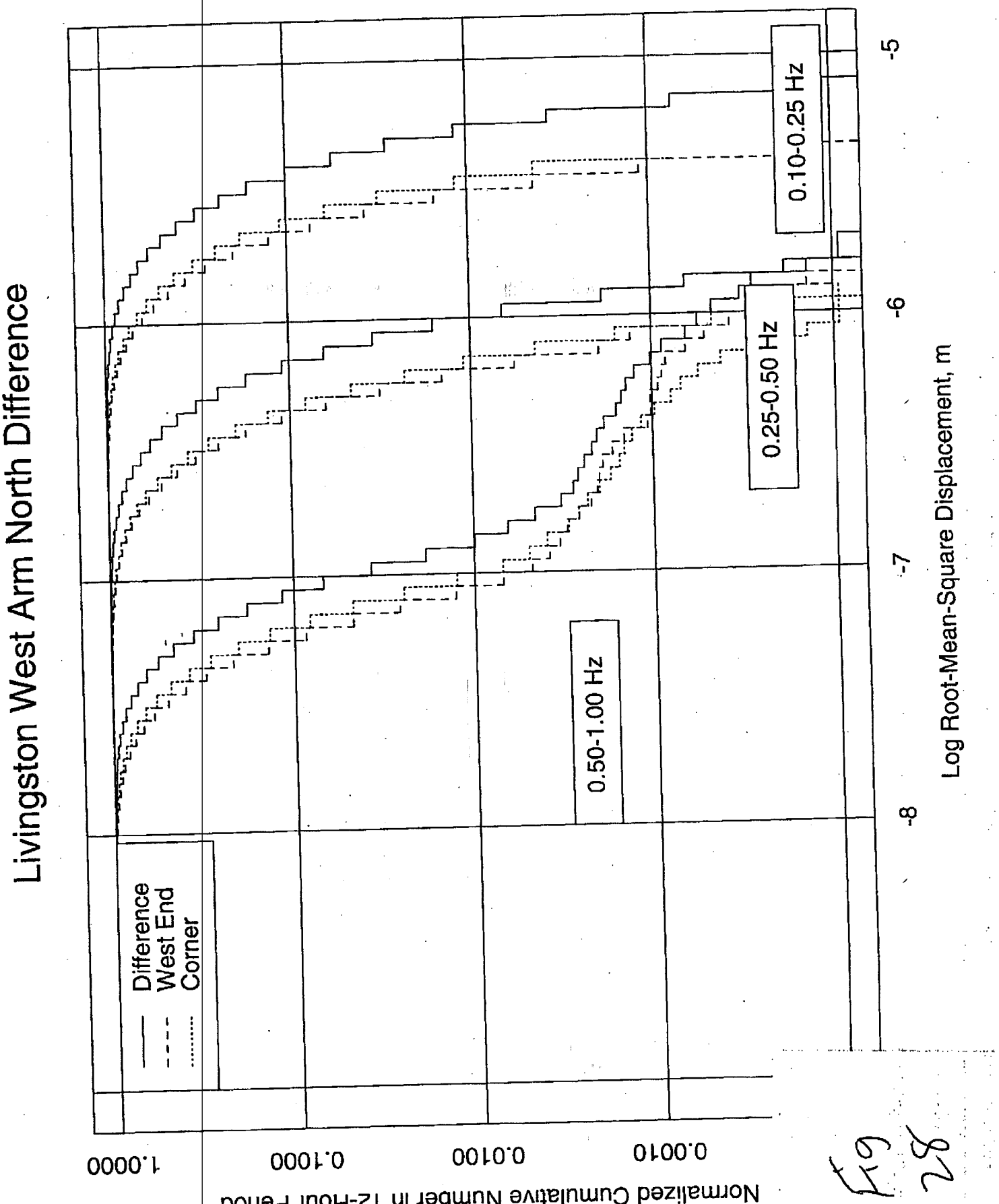
Livingston West Arm North Difference
Difference
West End
Corner
0.10-0.25 Hz
0.25-0.50 Hz
0.50-1.00 Hz
-5
-6
-7
-8
Log Root-Mean-Square Displacement, m
1.0000
0.1000
0.0100
0.0010
Normalized Cumulative Number in 12-Hour Period

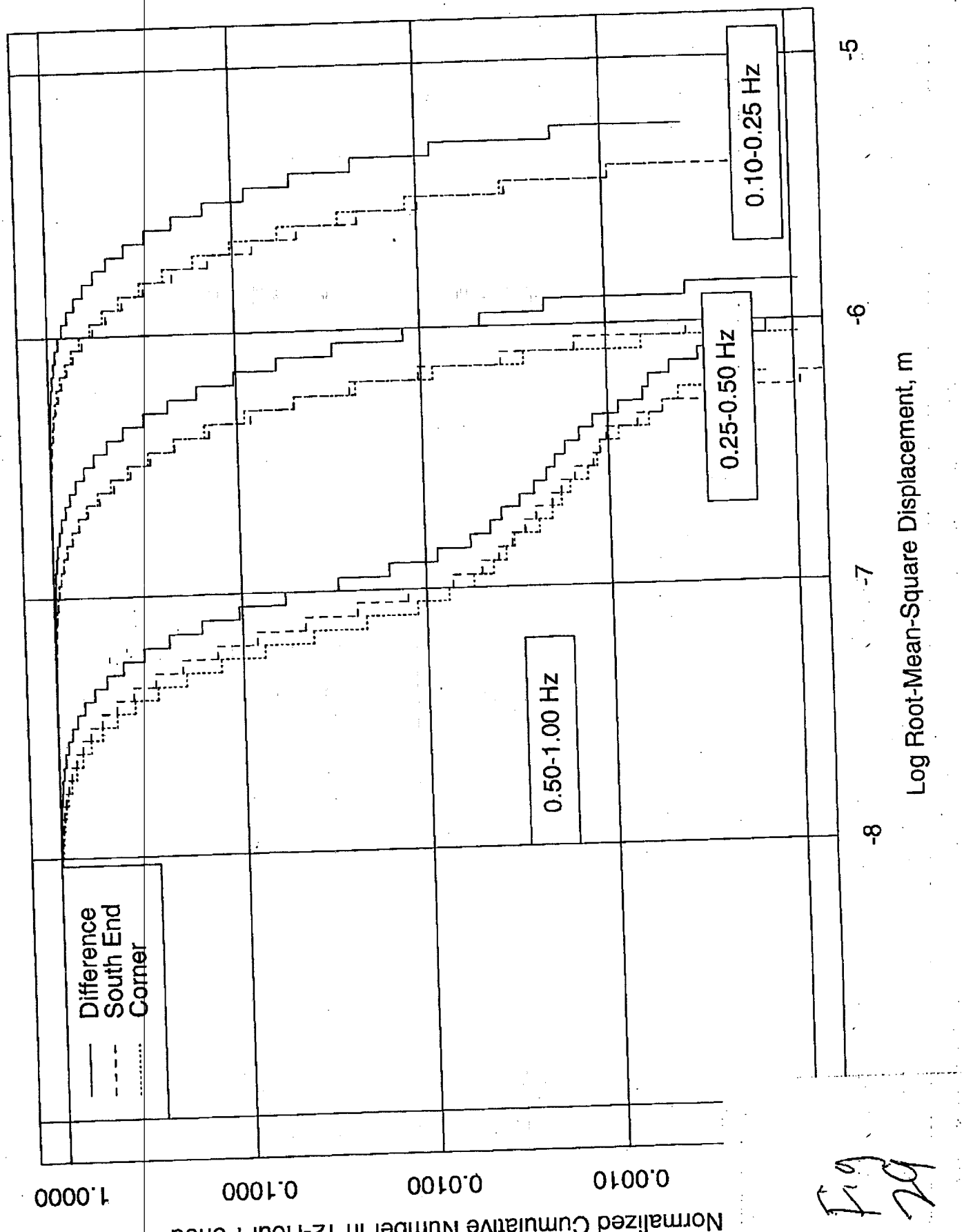
Livingston South Arm East Difference
Difference
South End
Corner
0.10-0.25 Hz
0.25-0.50 Hz
0.50-1.00 Hz
Normalized Cumulative Number in 12-Hour Period
1.0000
0.1000
0.0100
0.0010
Log Root-Mean-Square Displacement, m
-5
-6
-7
-8

Fig 29

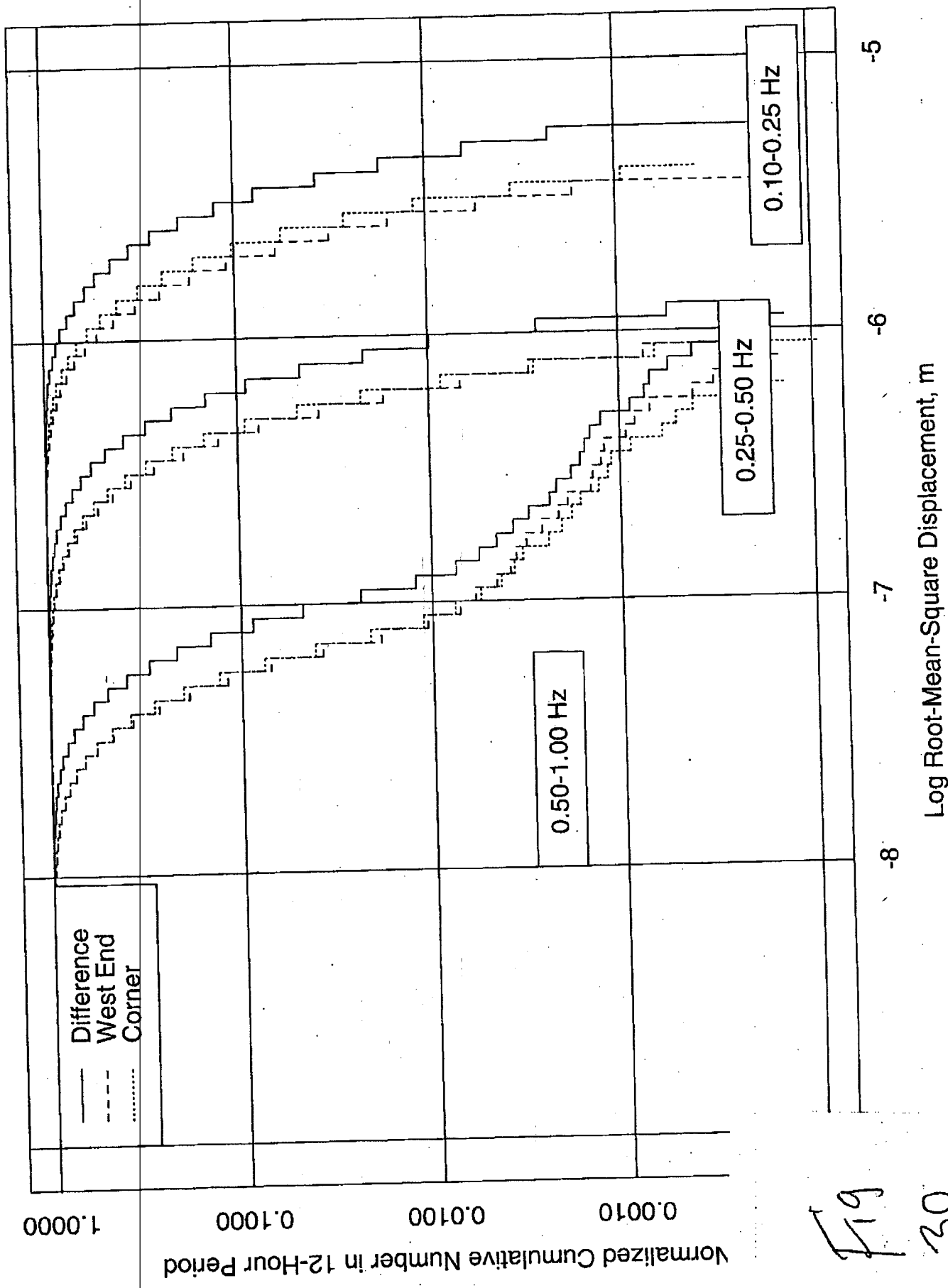
Livingston West Arm East Difference
Difference
West End
Corner
0.10-0.25 Hz
0.25-0.50 Hz
0.50-1.00 Hz
-5
-6
-7
-8
Log Root-Mean-Square Displacement, m
1.0000
0.1000
0.0100
0.0010
Normalized Cumulative Number in 12-Hour Period

F19
30

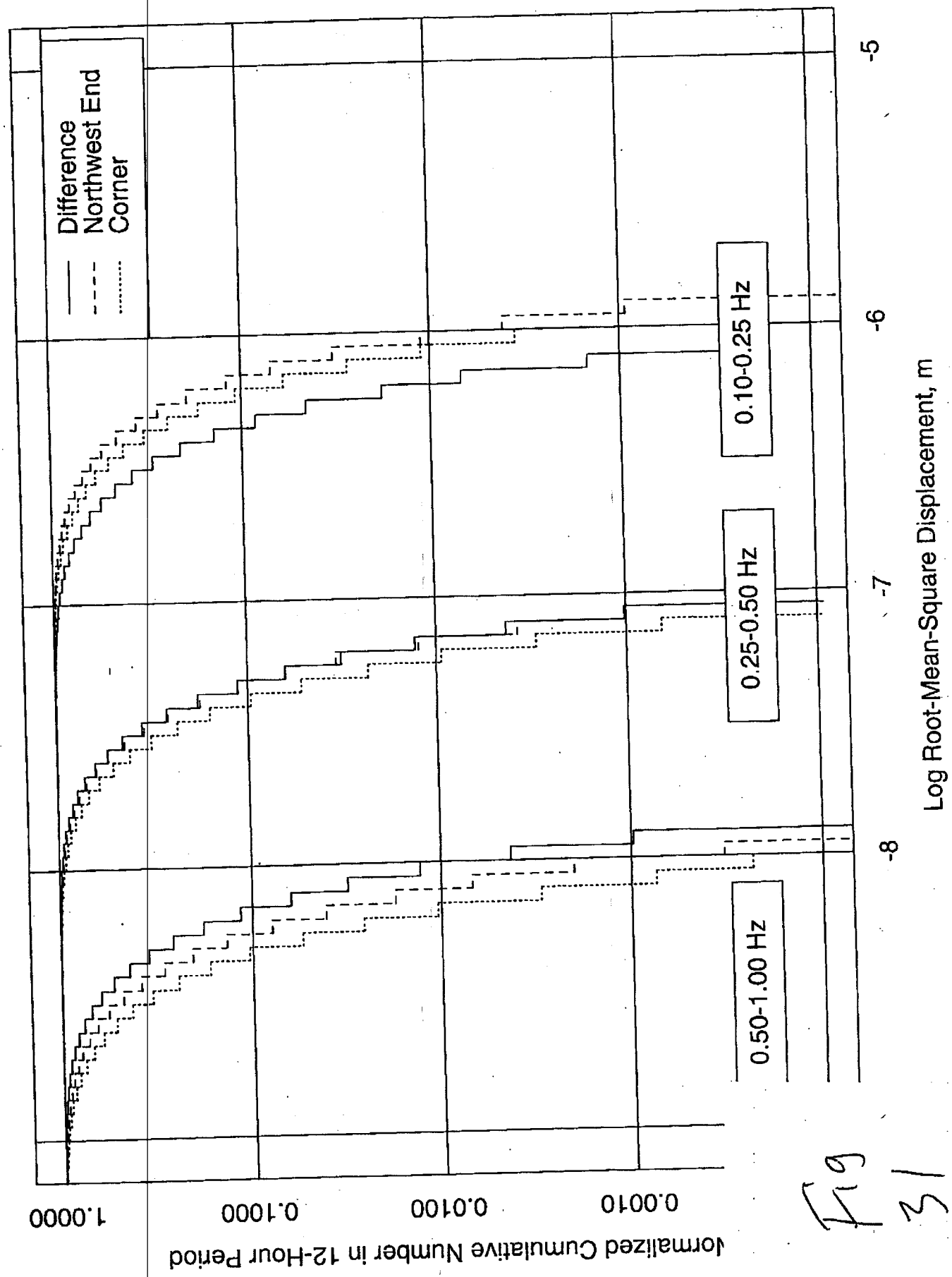
Hanford Northwest Arm Vertical Difference
Difference
Northwest End
Corner
0.10-0.25 Hz
0.25-0.50 Hz
0.50-1.00 Hz
Normalized Cumulative Number in 12-Hour Period
0.0010
0.0100
0.1000
1.0000
Log Root-Mean-Square Displacement, m
-5
-6
-7
-8

Fig 31

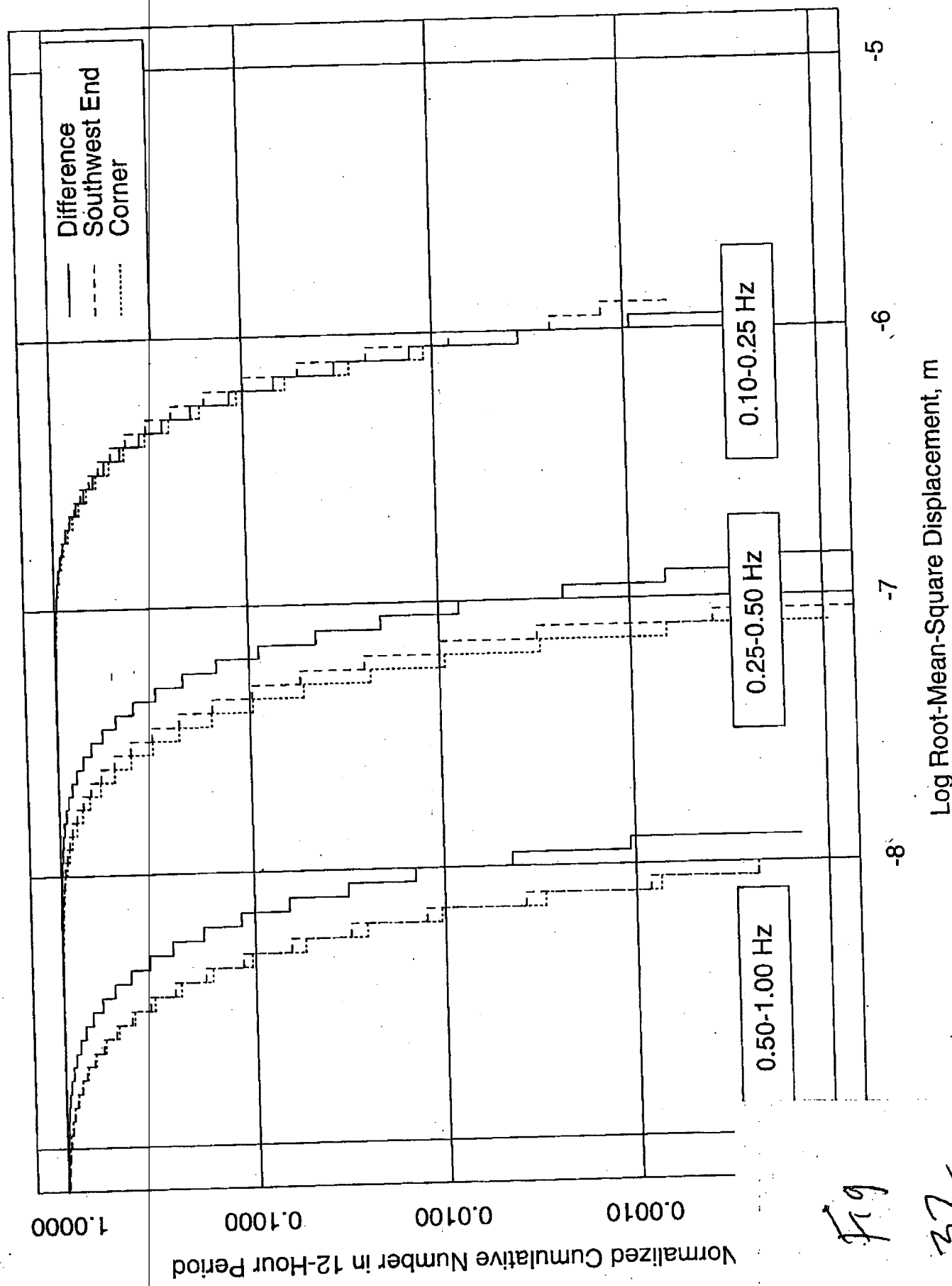
Hanford Southwest Arm Vertical Difference
Difference
Southwest End
Corner
0.10-0.25 Hz
0.25-0.50 Hz
0.50-1.00 Hz
Normalized Cumulative Number in 12-Hour Period
1.0000
0.1000
0.0100
0.0010
Log Root-Mean-Square Displacement, m
-5
-6
-7
-8

Fig 32

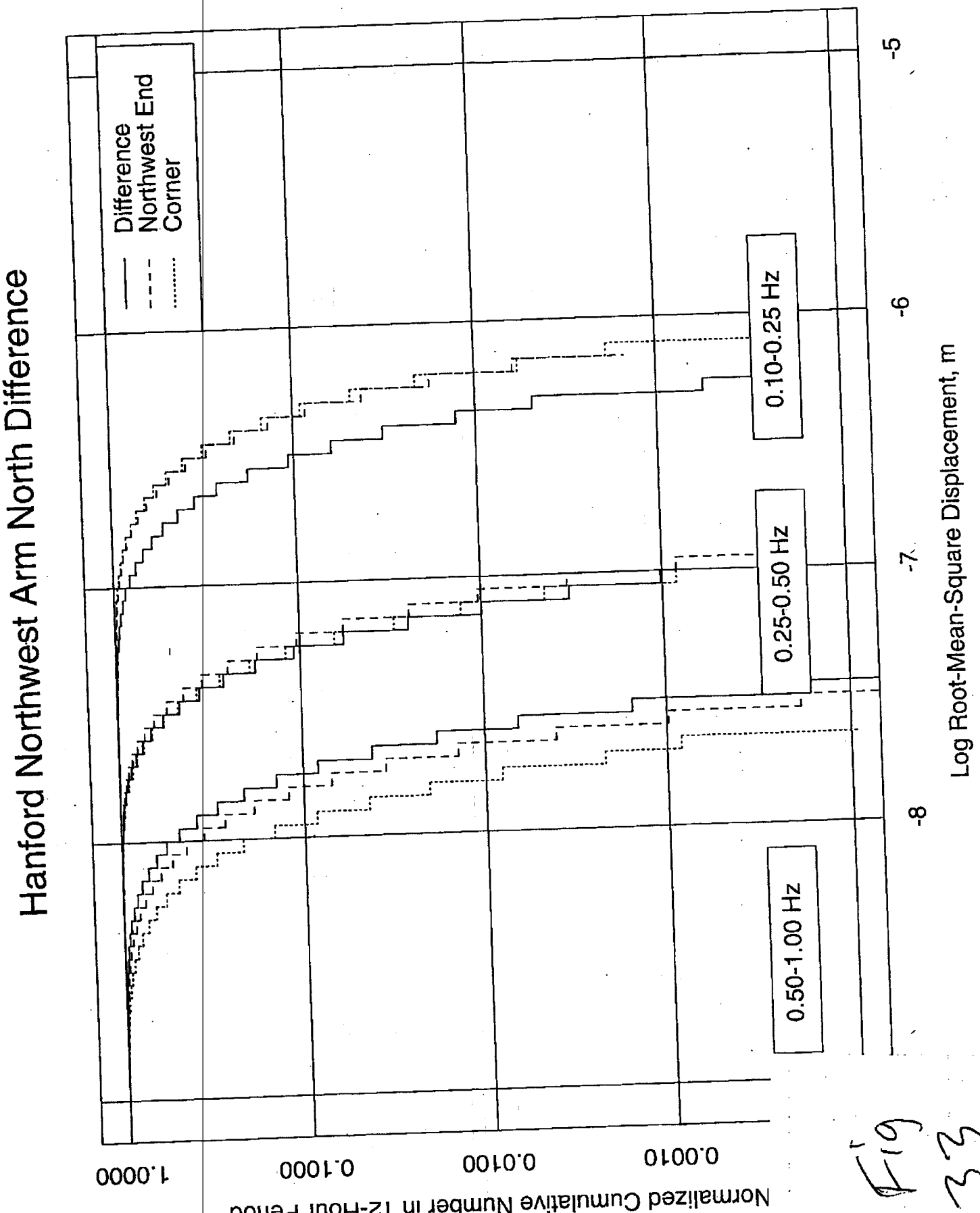
Hanford Northwest Arm North Difference
Difference
Northwest End
Corner
0.10-0.25 Hz
0.25-0.50 Hz
0.50-1.00 Hz
Normalized Cumulative Number in 12-Hour Period
0.0010
0.0100
0.1000
1.0000
Log Root-Mean-Square Displacement, m
-5
-6
-7
-8

F19
33

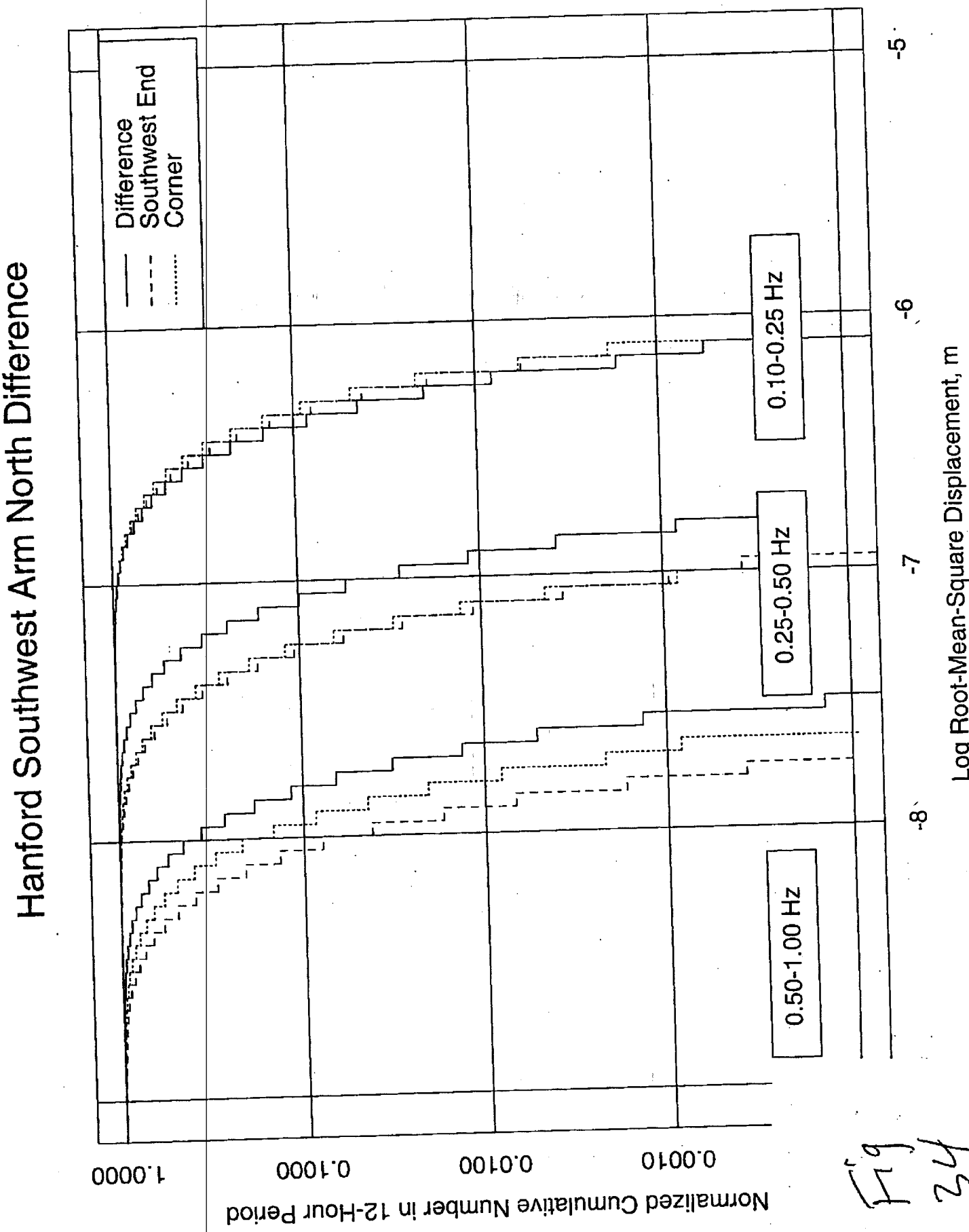
Hanford Southwest Arm North Difference
Difference
Southwest End
Corner
0.10-0.25 Hz
0.25-0.50 Hz
0.50-1.00 Hz
-5
-6
-7
-8
Log Root-Mean-Square Displacement, m
1.0000
0.1000
0.0100
0.0010
Normalized Cumulative Number in 12-Hour Period

Fig 24

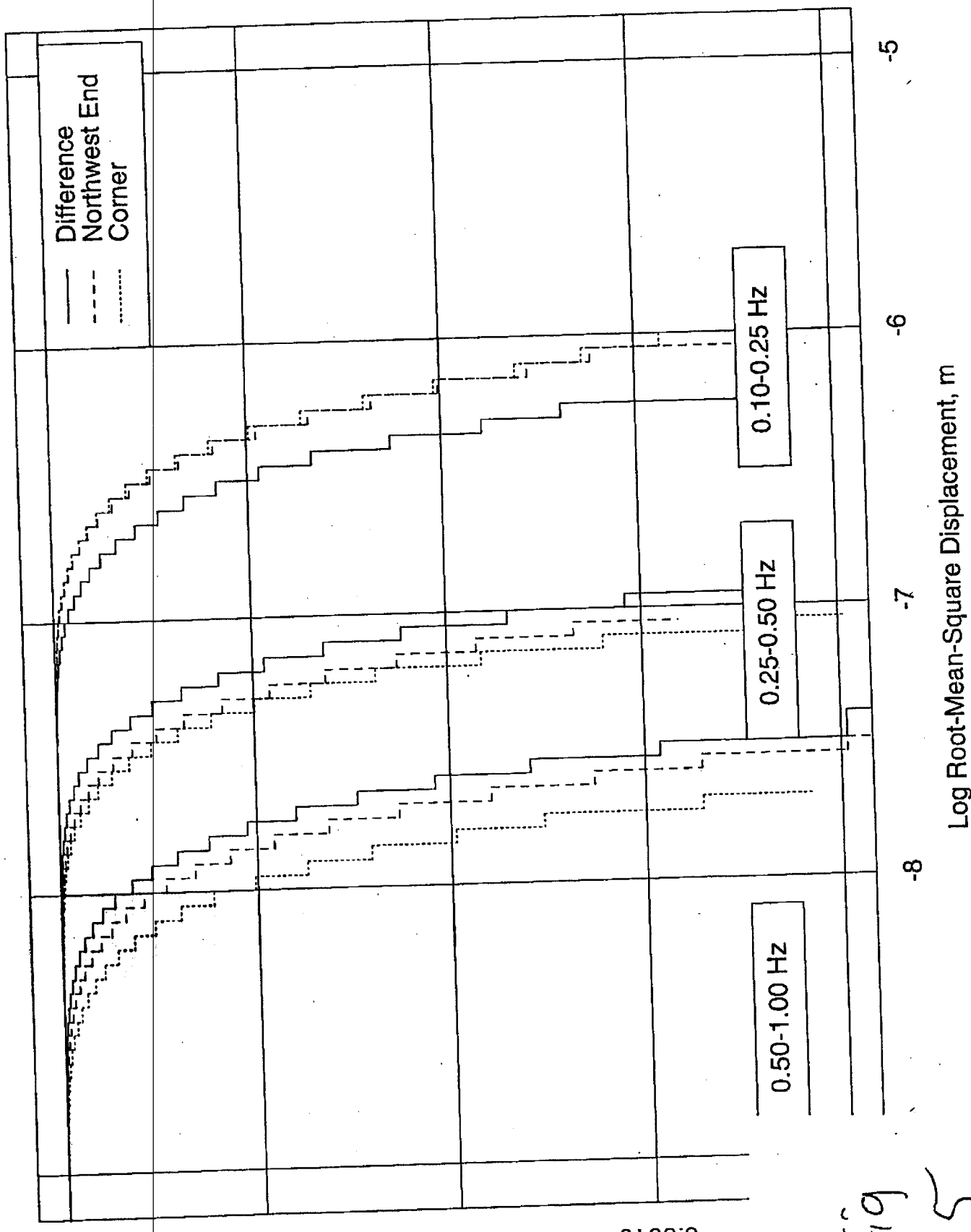
Hanford Northwest Arm East Difference
Difference
Northwest End
Corner
0.10-0.25 Hz
0.25-0.50 Hz
0.50-1.00 Hz
-5
-6
-7
-8
Log Root-Mean-Square Displacement, m
0.0010
0.0100
0.1000
1.0000
Normalized Cumulative Number in 12-Hour Period

Fig 35

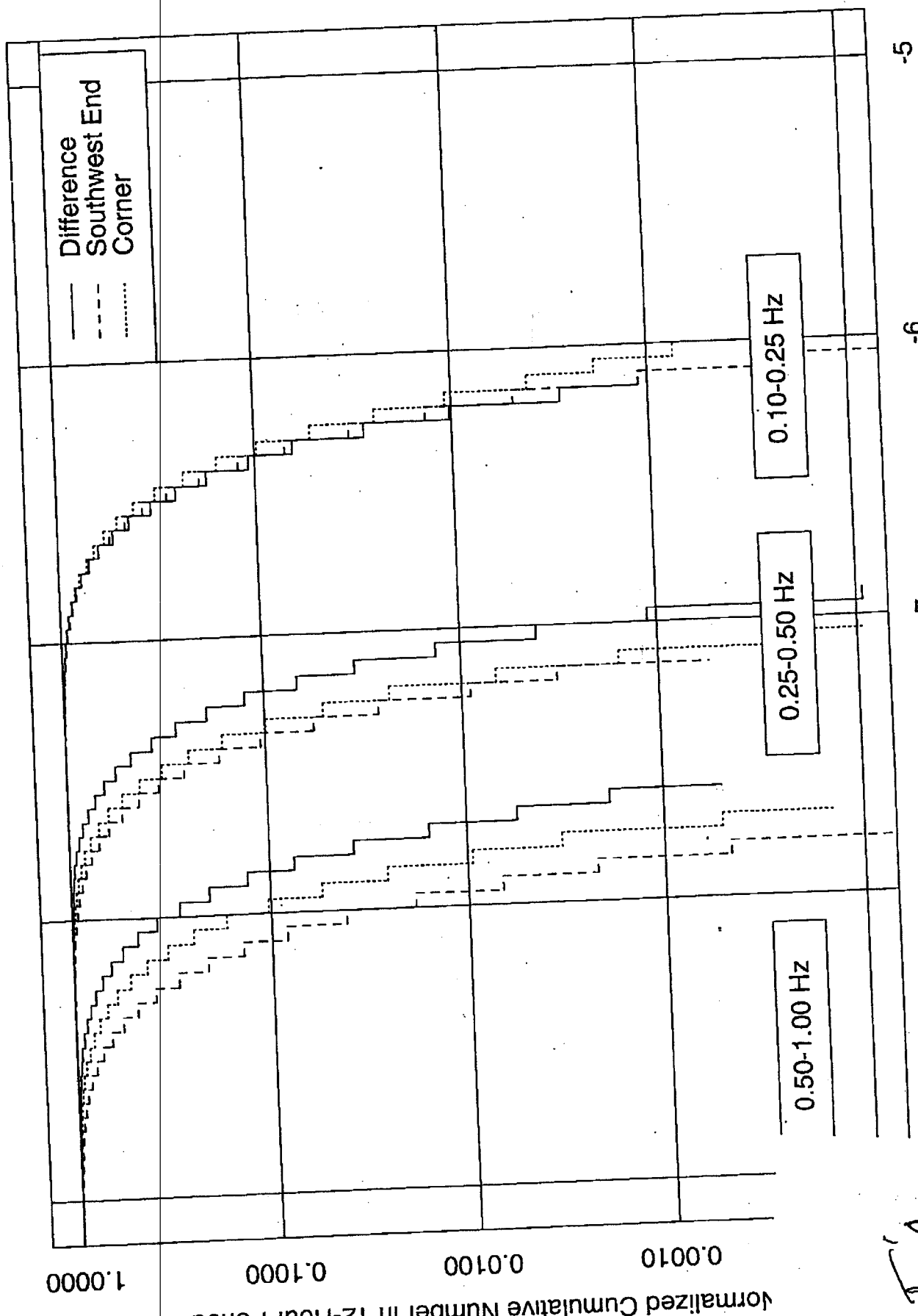
Hanford Southwest Arm East Difference
Difference
Southwest End
Corner
0.10-0.25 Hz
0.25-0.50 Hz
0.50-1.00 Hz
-5
-6
-7
-8
Log Root-Mean-Square Displacement, m
0.0010
0.0100
0.1000
1.0000
Normalized Cumulative Number in 12-Hour Period

Fig 36